Journal of Human Evolution 57 (2009) 484–502

Contents lists available at ScienceDirect

Journal of Human Evolution

journal homepage: www.elsevier.com/locate/jhevol

Geochronology of cave deposits at Liang Bua and of adjacent river terraces in the Wae Racang valley, western Flores, Indonesia: a synthesis of age estimates for the type locality of *Homo floresiensis*

R.G. Roberts [a,*], K.E. Westaway [a,f], J.-x. Zhao [b], C.S.M. Turney [a,g], M.I. Bird [c,h], W.J. Rink [d], L.K. Fifield [e]

[a] GeoQuEST Research Centre, School of Earth and Environmental Sciences, University of Wollongong, Wollongong, NSW 2522, Australia
[b] Radiogenic Isotope Laboratory, Centre for Microscopy and Microanalysis, Department of Earth Sciences, University of Queensland, Brisbane, Qld 4072, Australia
[c] School of Geography and Geosciences, University of St Andrews, St Andrews, Fife KY16 9AL, UK
[d] School of Geography and Earth Sciences, McMaster University, Hamilton, Ontario L8S 4K1, Canada
[e] Research School of Physical Sciences and Engineering, Australian National University, Canberra, ACT 0200, Australia
[f] Department of Environment and Geography, Division of Environmental Science, Macquarie University, North Ryde, NSW 2109, Australia
[g] Department of Geography, School of Geography, Archaeology and Earth Resources, University of Exeter, Exeter, EX4 4RJ, UK
[h] School of Earth and Environmental Sciences, James Cook University, Cairns, Qld 4870, Australia

ARTICLE INFO

Article history:
Received 18 January 2008
Accepted 21 January 2009

Keywords:
Quaternary geochronology
Numerical age estimates
Radiocarbon dating
Luminescence dating
Uranium-series dating
Electron spin resonance dating
Cave deposits
River terraces
Liang Bua
Wae Racang
Flores
Indonesia
Homo floresiensis

ABSTRACT

A robust timeframe for the extant cave deposits at Liang Bua, and for the river terraces in the adjoining Wae Racang valley, is essential to constrain the period of existence and time of extinction of *Homo floresiensis* and other biota that have been excavated at this hominin type locality. Reliable age control is also required for the variety of artifacts excavated from these deposits, and to assist in environmental reconstructions for this river valley and for the region more broadly. In this paper, we summarize the available geochronological information for Liang Bua and its immediate environs, obtained using seven numerical-age methods: radiocarbon, thermoluminescence, optically- and infrared-stimulated luminescence (collectively known as optical dating), uranium-series, electron spin resonance, and coupled electron spin resonance/uranium-series. We synthesize the large number of numerical age determinations reported previously and present additional age estimates germane to questions of hominin evolution and extinction.

Introduction

Archaeologists and physical anthropologists commonly require numerical age determinations for artifacts, human remains, and associated deposits to arrange the "target" objects or events in their correct temporal sequence. Numerical-age methods (following the terminology of Colman et al., 1987) are entirely or mostly self-contained, and produce quantitative age estimates that can be placed on a standard timescale. The resultant ages are typically expressed in years before present, with an error term that indicates the degree of uncertainty associated with the age estimate. Recent reviews are provided in Walker (2005), Wintle (2007), and Roberts and Jacobs (2008).

The excavations of the cave deposits at Liang Bua from 2001 to 2004 involved the collection of samples for dating by a variety of numerical-age methods, including radiocarbon (^{14}C), luminescence – a collective term for the related techniques of thermoluminescence (TL), optically-stimulated luminescence (OSL), and infrared-stimulated luminescence (IRSL) – uranium-series (U-series, specifically ^{230}Th/^{234}U), and electron spin resonance (ESR), the latter coupled with U-series. We applied this range of dating methods which are (based on different physical principles) to diverse materials (of different origin) so that problems with any particular method or material could be identified before the final

* Corresponding author.
E-mail address: rgrob@uow.edu.au (R.G. Roberts).

0047-2484/$ – see front matter © 2009 Elsevier Ltd. All rights reserved.
doi:10.1016/j.jhevol.2009.01.003

ages were determined for the objects and events of interest. Such quality-assurance measures are necessary for the construction of accurate chronologies, which became of paramount importance with the discovery of the holotype of *Homo floresiensis* (LB1) in September 2003. Robust numerical ages are also needed for the associated stone artifacts and other faunal remains recovered from these excavations, to provide chronological control for the Liang Bua stratigraphy and for reconstructions of the prevailing environmental conditions in and around this cave.

This paper reviews the geochronological investigations conducted since 2001 on the cave deposits at Liang Bua and on the nearby river terraces in the Wae Racang valley. We summarize all numerical age determinations, including those reported previously as well as several unpublished age estimates (see Table 1 for a complete listing), which are of relevance to the archaeology, palaeontology, and palaeoenvironmental context of the discoveries made at Liang Bua. The stratigraphy and sedimentology of the cave deposits are described by Westaway et al. (2009a), and details of the river terrace deposits are given in Westaway et al. (2009b).

Study sites and sample collection

An extensive series of samples (85 in total) has been analyzed from Liang Bua and its environs; more have been collected but not analyzed. This total consists of 26 sediment samples for luminescence dating (several of which have been dated by more than one luminescence technique), 22 samples of speleothem for U-series dating, 25 charcoal samples for accelerator mass spectrometry (AMS) ^{14}C dating (some of which have been dated from more than one temperature fraction), and 12 teeth (*Stegodon* molars) for ESR dating (two of which have also been dated by U-series to obtain "coupled" ESR/U-series ages).

Samples for dating by all of the above methods have been collected from several excavated Sectors throughout the cave and from the conglomerate deposit at the rear of the cave (Figs. 1 and 2) to constrain the ages of the buried artifacts and faunal remains, especially those of *Homo floresiensis*. Samples for TL and OSL dating have also been collected from the river terraces T3, T4, and T5, located outside the cave entrance in the Wae Racang valley; site details are given in Westaway et al. (2009b). U-series samples U21 and U22 were collected from the top and bottom of a stalagmite (SPI-1) formed in a small cave situated ~90 m above, and connected to, Liang Bua; this remnant cave is referred to as "Outcrop I" in Westaway et al. (2009b).

The remains of LB1 were found at a depth of 5.9 m in Sector VII, at the same level as TL/IRSL sample LBS7-42 (denoted as L13 in Fig. 2d) and ^{14}C samples ANUA-27116 and ANUA-27117 (shown as C17 and C18 in Fig. 2d). All of the samples reported here were collected during the course of the 2001–2004 excavations at Liang Bua, except for 9 radiocarbon samples (C3–10 and C12) collected from earlier excavations by R.P. Soejono (Morwood et al., 2009). The latter samples originate from the upper ~3 m of deposit in Sector IV, and are reported here to provide a complete account of all known numerical age determinations at Liang Bua.

Samples were collected using standard procedures for each dating method. For ^{14}C dating, the excavated cave deposits were placed in plastic bags and immediately sealed. Scattered charcoal fragments were subsequently hand-picked in the laboratory for analysis. These fragments were recovered from the material excavated from individual spits and retained on 2 mm sieve mesh (i.e., not directly from the cleaned walls or floor of an excavation), so their locations can be fixed vertically to within ± 10 cm (the thickness of a typical spit) and horizontally to within ± 25 cm (the planform dimensions of a typical bucket-load of deposit). We did not attempt direct ^{14}C dating of bone collagen from LB1, because this would have resulted in partial destruction of the holotype of a new hominin species with only a low chance of success, given that collagen is unlikely to have been preserved in the tropical weathering environment.

Sediment samples for luminescence dating were collected by hammering opaque plastic tubes into the cleaned section walls, and then removing and sealing the tubes to prevent light exposure and mixing of the sediments, and to retain their field moisture contents. The empty tube holes were then enlarged and a portable gamma-ray spectrometer inserted to obtain *in situ* measurements of the gamma dose rate at the sampling locations. Quartz and potassium-rich feldspar grains were extracted from the bulk sediments for TL/OSL and IRSL dating, respectively, under safelight conditions in the laboratory. Quartz and feldspar grains were also extracted from a burnt pebble found at a depth of 8.4 m in Sector VII (Morwood et al., 2005). When collected, the pebble was immediately wrapped in light-proof black plastic and the gamma dose rate was measured at the find spot (marked as L14 in Fig. 2d). At each location, an additional sample of sediment was collected and sealed in a plastic bag for laboratory determinations of radioactivity and moisture content. Full details are given in Westaway (2006).

Samples of calcite for U-series dating were collected by removing chunks of speleothem from subaerially-exposed and buried flowstones using a hammer and chisel, and then sealing them in plastic bags for later preparation and analysis in an ultra-clean laboratory environment.

Whole *Stegodon* molars and fragments of molar were collected for ESR dating. Four of these teeth were recovered directly from the deposit during excavation (denoted as E5, E7, E9, and E12 in Fig. 2c), so their locations are known to the nearest cm; field gamma-ray spectrometry measurements were made at each of these find spots. The other 8 teeth were collected from the material excavated from individual spits and retained on 2 mm sieve mesh, so their stratigraphic positions are constrained with the same precision as the ^{14}C samples. For the latter ESR samples, gamma dose rates were estimated from measurements made in the same stratigraphic layer, from as close as possible to the excavated spit. The teeth were deliberately not cleaned in the field, so that accurate estimates could be made of the external beta dose rate from the adhering sediment. U-series dating of the enamel and dentine was also conducted on three of the whole teeth – LB-JR-8A (a juvenile *Stegodon* molar with dimensions of 4 cm × 2 cm × 2 cm, plotted as E5 in Fig. 2c) and two adult molars (LB-JR-14B and LB-JR-15A) – to test for U loss and obtain combined (or "coupled") ESR/U-series ages for suitable samples (Grün et al., 1988; Rink, 1997; Grün, 2006, 2007). The field moisture content of the deposits surrounding each of the ESR samples was determined from the additional sediment samples collected for luminescence dating.

Dating techniques, equipment, and procedures

Radiocarbon dating

Eleven charcoal samples ("ANUA-" in Table 1) were prepared using acid–base wet oxidation (ABOX) ^{14}C procedures and then step-combusted at 330 °C, 650 °C, and either 850 °C or 910 °C in a vacuum line insulated from atmospheric contamination by a secondary backing vacuum (Bird et al., 1999). Previous studies have shown that most contamination is removed at the 330 °C combustion step, so that greatest confidence can be placed in ^{14}C ages obtained from the fractions combusted at temperatures of 850 °C and higher (e.g., Bird et al., 1999, 2002, 2003; Fifield et al., 2001; Turney et al., 2001; Bird, 2007). Graphite targets were

Table 1
List of ^{14}C (C), uranium-series (U), luminescence (L), and electron spin resonance (E) samples collected from Liang Bua and the neighboring caves and river terraces.

Figure code[a]	Sample code[b]	Sampling location[c]	Dating technique[d]	Age[e] (ka)	Reference source[f]
C1	ANUA-23607	Sector III	^{14}C	1.82–0.94	7
C2	ANUA-23610	"	"	17.1–15.7	1
C3	GrN-15870	Sector IV	"	0.28–0.00	7
C4	GrN-15871	"	"	0.63–0.50	7
C5	GrN-14301	"	"	0.51–0.33	7
C6	GrN-14302	"	"	0.66–0.49	7
C7	GrN-15872	"	"	0.54-0.31	7
C8	GrN-14303	"	"	0.53–0.33	7
C9	GrN-14304	"	"	4.41–2.95	7
C10	GrN-14305	"	"	4.51–3.84	7
C11	ANUA-19207	"	"	6.67–6.02	5
C12	GrN-14306	"	"	12.8–10.0	7
C13	ANUA-19206	"	^{14}C (650)	10.2–9.5	5
"	ANUA-19214	"	^{14}C (910)	9.5–8.7	7
C14	ANUA-19209	"	^{14}C (650)	11.4–10.4	1
"	ANUA-19211	"	^{14}C (910)	11.2–10.2	1
C15	ANUA-19203	"	^{14}C (650)	17.1–15.8	1
"	ANUA-19210	"	^{14}C (910)	17.4–15.9	1
C16	ANUA-27115	Sector VII	^{14}C	13.4–12.7	1
C17	ANUA-27116	"	"	19.0–17.9	1
C18	ANUA-27117	"	"	18.7–17.1	1
C19	ANUA-31229	"	"	19.7–18.2	7
C20	ANUA-32717	"	"	19.8–18.9	7
C21	Wk-16351	Sector XI	"	0.26–0.03	7
C22	Wk-16352	"	"	0.54–0.48	7
C23	Wk-16353	"	"	2.84–2.62	5
C24	Wk-16354	"	"	5.30–4.98	7
C25	Wk-16355	"	"	8.37–8.19	7
U1	LB-03-1/45–49	Sector I	U-series	48.8 ± 0.3	5
U2	LB-03-1/7–12	"	"	53.3 ± 0.3	5
U3	LB-03-2/2–13	"	"	61.0 ± 2.4	5
U4	LB-17-A2/48–52	Sector III	"	140 ± 4	7
U5	LB-17-A2/21–27	"	"	225 ± 31	7
U6	LB-17-A2/3–8	"	"	374 ± 30	4
U7	LB-JR-6A/13–23	Sector IV	"	37.7 ± 0.2	1
U8	BERT#5	West wall	"	43.3 ± 0.3	7
U9	BERT#6	"	"	14.8 ± 0.3	7
U10	BERT#7	"	"	58.6 ± 0.5	7
U11	LB-JR-10A/20–25	Conglomerate	"	87.6 ± 0.6	4
U12	LB-JR-10B/75–80	"	"	96.8 ± 0.6	4
U13	LB-JR-10B/3–8	"	"	102.4 ± 0.6	1
U14	LB-JR-11A/15–15	"	"	88 ± 9	4
U15	LB-JR-12/10–15	"	"	58.6 ± 0.5	7
U16	LB-CON-F2	"	"	47 ± 12	4
U17	LB-CP2-F1-top	"	"	46.5 ± 0.5	4
U18	LB-CP2-F1-base	"	"	48.5 ± 1.7	4
U19	LB-CP3-F2-matrix	"	"	46.3 ± 2.0	4
U20	LB-CP3-F2-clast	"	"	76.2 ± 0.5	7
U21	SPI-1-top	Outcrop I	"	74.9 ± 0.6	5
U22	SPI-1-base	"	"	88.8 ± 0.8	5
L1	LBS1-16	Sector I	TL	52 ± 20	5
"	LBS1-16	"	OSL	$75\ ^{+12}/_{-10}$	5
L2	LBS1-12	"	TL	55 ± 49	5
"	LBS1-12	"	OSL	$87\ ^{+11}/_{-12}$	5
L3	LBS3-4	Sector III	TL	69 ± 12	5*
L4	LBS3-2	"	"	106 ± 31	5*
L5	LBS4-3	Sector IV	"	71 ± 6*	5
L6	LBS4-34	"	"	70 ± 8	5
L7	LBS4-30	"	"	14 ± 3	5
L8	LBS4-1	"	"	131 ± 10*	5
L9	LBS4-26	"	"	65 ± 25	5
L10	LBS4-28	"	"	110 ± 20	4
L11	LBS4-32	"	"	95 ± 13	1
L12	LBS7-40	Sector VII	"	40 ± 8	5*
"	LBS7-40	"	IRSL	14 ± 2	1
L13	LBS7-42	"	TL	36 ± 5	5*
"	LBS7-42	"	IRSL	6.8 ± 0.8	1
L14	LBS7-44	"	TL	370 ± 156*	5
"	LBS7-44	"	IRSL	263 ± 43	5
L15	LBS7-46	"	TL	41 ± 10	2
L16	LBS7-45	"	"	55 ± 8	2
L17	LBS11-50	Sector XI	"	37 ± 21*	5
L18	LBC-37	Conglomerate	"	130 ± 57	4*
L19	LBC-36	"	"	193 ± 33	4*
L20	WR-9	Terrace 3	"	340 ± 17*	3
L21	WR-14	"	"	97 ± 8	6
"	WR-14	"	OSL	$140\ ^{+24}/_{-14}$	6
L22	WR-15	"	TL	118 ± 48	4
"	WR-15	"	OSL	$97\ ^{+15}/_{-16}$	6
L23	WR-13	Terrace 4	TL	18 ± 4	6
"	WR-13	"	OSL	36 ± 7	6
L24	LB-48	"	TL	608 ± 58*	6
"	LB-48	"	OSL	31 ± 5	6
L25	LB-47	"	TL	356 ± 24*	6
L26	WR-1	Terrace 5	"	5 ± 2	6*
"	WR-1	"	OSL	$26\ ^{+9}/_{-3}$	6
E1	LB-JR-30A	Sector I	ESR	22–37	7
E2	LB-JR-35A	Sector IV	"	23–36	7
E3	LB-JR-9A	"	"	34–57	7
E4	LB-JR-12A	"	"	32–56	7
E5	LB-JR-33A	"	"	20–29	7
E6	LB-JR-8A	"	"	54–91	1
"	LB-JR-8A	"	ESR/U-series	$74\ ^{+14}/_{-12}$	1
E7	LB-JR-34A	"	ESR	32–53	7
E8	LB-JR-14B	"	"	58–92	7
"	LB-JR-14B	"	ESR/U-series	$154\ ^{+17}/_{-13}$	7
"	LB-JR-14D	"	ESR	42–69	7
E9	LB-JR-31B	"	"	36–52	7
E10	LB-JR-32A	"	"	35–53	7
E11	LB-JR-15A	"	"	40–70	7
"	LB-JR-15A	"	ESR/U-series	nd	7
E12	LB-JR-36A	Sector VII	ESR	26–44	7

[a] Refers to sample locations shown in Figs. 1 and 2.
[b] Refers to sample codes assigned by dating laboratory.
[c] See Fig. 1 for "Sector," "Conglomerate," and "West wall" locations, and Westaway et al. (2009b) for locations of "Terrace" and "Outcrop I" samples.
[d] Combustion temperatures (in °C) are shown in parentheses for charcoal samples from which separate ^{14}C age were estimated from more than one fraction. Thermoluminescence (TL) and optically-stimulated luminescence (OSL) techniques were applied to the light-sensitive signals in quartz sediments, and potassium-rich feldspars were dated by means of infrared-stimulated luminescence (IRSL). U-series refers to the ^{230}Th/^{234}U dating of speleothem, and ESR/U-series dating refers to the modelled ages obtained from combined electron spin resonance (ESR) and ^{230}Th/^{234}U dating of enamel from the same *Stegodon* tooth. ESR samples LB-JR-14B and LB-JR-14D are different enamel fragments of the same adult molar.
[e] Expressed in thousands of calendar years (ka), with the ^{14}C ages calibrated using IntCal04 and a Southern Hemisphere offset of 40 ± 13 years. The ^{14}C age ranges and the U-series uncertainties are given at the 95% confidence interval, whereas the luminescence, ESR, and coupled ESR/U-series ages are given at the 68% confidence interval, following conventions for each of these methods. The ESR age ranges are shown as EU–LU, where EU and LU represent model assumptions of early and linear U-uptake, respectively. Only TL ages obtained using the bleachable red TL signal are listed, except for the 7 samples marked with an asterisk (*), which could only be dated using the light-insensitive (heat-reset) signal. The abbreviation "nd" specifies that U-loss was indicated for this sample, so a combined ESR/U-series age could not be determined.
[f] 1, Morwood et al. (2004); 2, Morwood et al. (2005); 3, Westaway and Roberts (2006); 4, Westaway et al. (2007b); 5, Westaway (2006); 6, Westaway et al. (2009b); 7, this study. We have calibrated all ^{14}C ages using the latest internationally-ratified calibration data set (IntCal04), so some of the calibrated ages differ trivially from those cited in Morwood et al. (2004). Seven of the TL ages (indicated by asterisks) also differ slightly from those published originally by Morwood et al. (2004) and by Westaway and Roberts (2006), owing to the incorporation of additional TL data, revised water contents, and updated dose-rate conversion factors. The ^{14}C and TL ages listed here are considered more accurate than the original estimates, and supersede them.

produced from the carbon dioxide evolved at the 650 °C and 850 °C or 910 °C steps, and the ^{14}C/^{13}C ratios were measured by AMS using the 14UD accelerator at the Australian National University.

The 5 charcoal samples coded "Wk-" were pre-treated at the University of Waikato using conventional acid–base–acid (ABA)

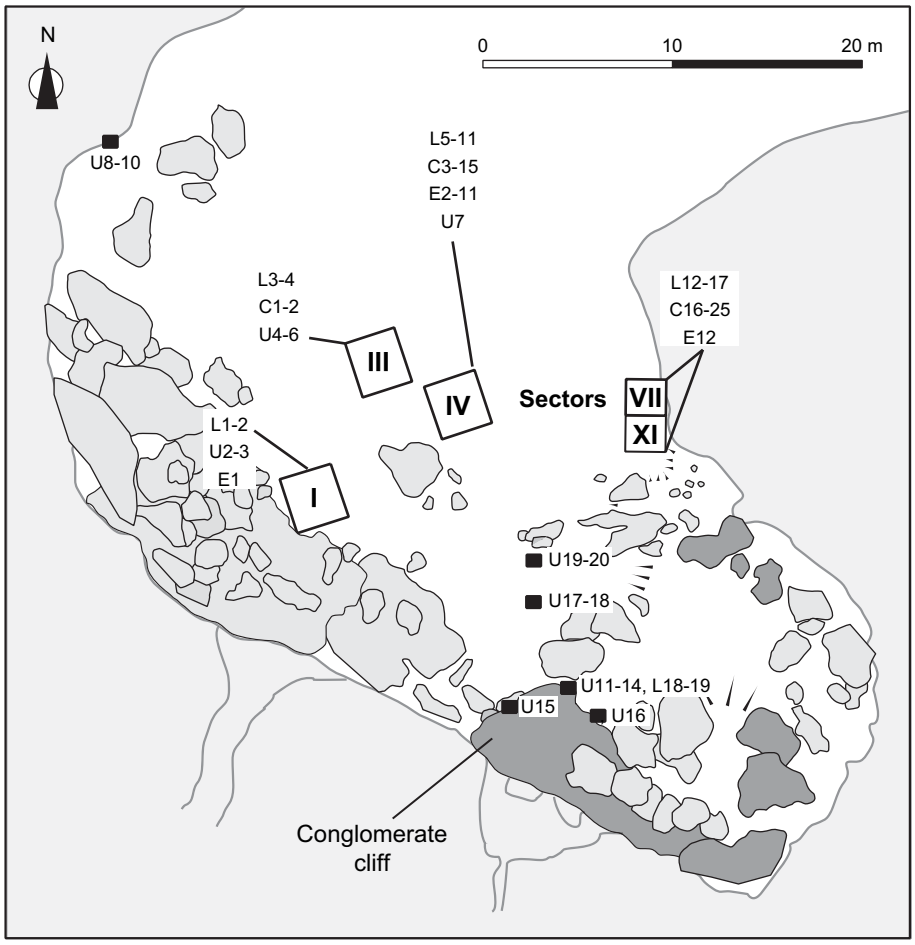

Figure 1. Plan of Liang Bua, showing the locations of the dated archaeological excavations (Sectors I, III, IV, VII, and XI) and conglomerate deposits at the rear of the cave (dark grey shading). Flowstone and stalagmite accumulations are shaded in medium grey, and the surrounding limestone cave walls in light grey. Locations of ^{14}C (C), uranium-series (U), luminescence (L), and electron spin resonance (E) samples are also shown, along with the corresponding code numbers referred to in Fig. 2 and Table 1.

procedures, converted to graphite, and measured by AMS at the Rafter Radiocarbon Laboratory in New Zealand; the only exception was sample Wk-16353, which was converted to benzene and measured by liquid scintillation counting at Waikato. The remaining 9 charcoal samples (GrN) were prepared and measured at the University of Groningen in the Netherlands. Samples GrN-14302 to GrN-14306 were pre-treated with acid only, whereas the other samples were given the full ABA pre-treatment. For each of the Groningen samples, the organic residue was converted to carbon dioxide and dated by gas-proportional beta counting. The use of multiple laboratories provides the opportunity to assess the extent of coherence among ^{14}C age estimates obtained for charcoal samples subjected to a variety of pre-treatments and measured using a range of alternative techniques.

All conventional ages (i.e., the measured ages, expressed in radiocarbon years before present, BP) included a correction for carbon-isotope fractionation based on the measured δ^{13}C value for each sample (range $-24.8‰$ to $-29.6‰$) or an assumed value of $-25.0‰$ for charcoal. We calibrated these ages using the IntCal04 dataset and Calib5.0 (Reimer et al., 2004), with a Southern Hemisphere offset of 40 ± 13 years (Hogg et al., 2002). The 68% and 95% confidence intervals for the calibrated ages are listed in Table 1; henceforth in this paper, we refer exclusively to calibrated ^{14}C ages, which are expressed in calendar years and are, therefore, directly comparable to the numerical ages obtained from luminescence, U-series, and ESR dating.

Uranium-series dating

Unaltered calcite crystals were extracted from each of the 22 samples of speleothem by removing any weathered surfaces and then breaking the cleaned sample into small pieces. Fragments with a shiny, crystalline appearance were cleaned ultrasonically and spiked with a ^{229}Th–^{233}U–^{236}U mixed tracer. The precisely-known ^{233}U/^{236}U ratio was used to monitor and correct for U mass-fractionation to improve the analytical precision of the measured U-isotope ratios for the speleothem samples. After total dissolution in nitric acid, concentrated hydrogen peroxide was added to decompose any organic matter and to ensure complete mixing between the spike and the sample. U and Th were co-precipitated with iron hydroxide, and then redissolved in nitric acid prior to purification using standard anion-exchange methods.

The U and Th fractions were loaded on to individual, pre-treated rhenium filaments and sandwiched between two graphite layers. The U and Th isotope signals were measured as ^{232}Th/^{229}Th, ^{229}Th/^{230}Th, ^{233}U/^{235}U, ^{234}U/^{235}U, and ^{233}U/^{236}U ratios by thermal ionization mass spectrometry (TIMS) at the University of Queensland. These ratios were converted to U and Th concentrations by taking into account the mass of each sample and the mixed tracer, and the U and Th concentrations of the latter. The ^{230}Th/^{238}U and ^{234}U/^{238}U activity ratios were then estimated by comparison with the corresponding ratios obtained from repeat analyses of the international HU-1 uraninite standard.

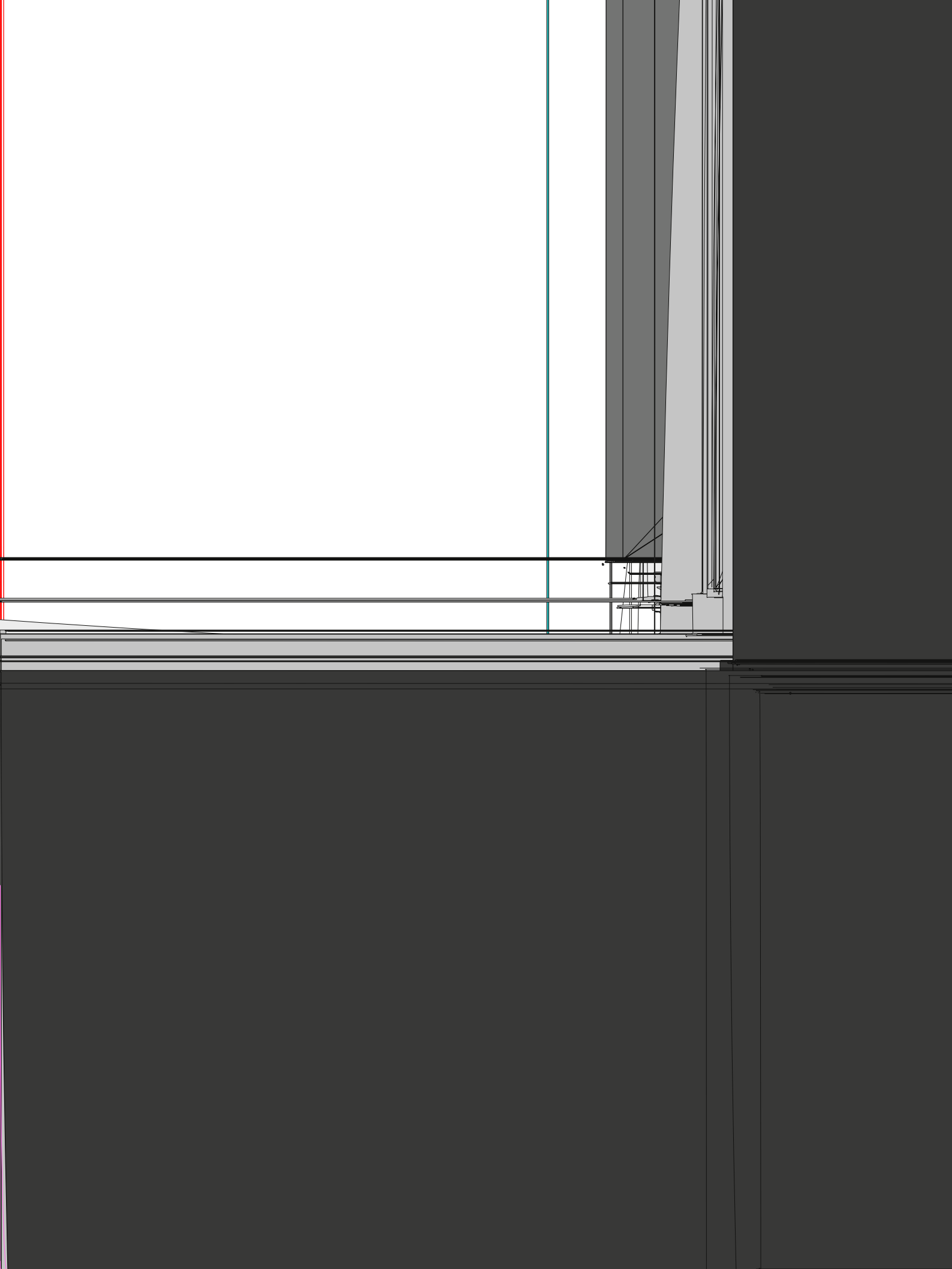

sequential treatments in hydrochloric acid (to dissolve carbonates), hydrogen peroxide (to remove organic matter), and sodium hydroxide (to disperse clay aggregates), followed by sieving to isolate K-feldspar grains of 125–212 μm in diameter and quartz grains of this size or smaller (90–125 μm). The coarser quartz fraction was used for all single-grain OSL analyses and for TL dating of four of the fluvially-transported samples (L18, L21, L24, and L26 in Table 1). Heavy minerals were removed using a sodium polytungstate solution with a specific gravity of 2.70, followed by separations of quartz, Na-feldspar, and K-feldspar grains using solutions with specific gravities of 2.62 and 2.58 (Aitken, 1998). The external, alpha-irradiated portions of these grains were removed by etching with 40% hydrofluoric acid for 45 min (quartz) or 10% acid for 10 min (feldspar), and given a final rinse in hydrochloric acid to dissolve any precipitated fluorides. In the case of the burnt pebble, its charred surface was first scraped clean and three thin layers were successively removed. Quartz and feldspar grains were obtained (as above) from these outermost layers, which are the most likely to have been burnt with sufficient intensity to have emptied the electron traps that give rise to the TL and IRSL signals. Further details on all aspects of the luminescence dating investigations are given in Westaway (2006).

For TL dating, quartz grains were mounted on to stainless-steel discs, using silicone oil as an adhesive, with each disc (aliquot) consisting of ~5000 grains. TL measurements were made of the red emissions (rather than the conventional blue signal, which could not be detected in these samples), using two different photomultiplier tubes (Electron Tubes Ltd 9235QA and S20 9658B, the latter cooled to −20 °C). To estimate the time elapsed since the grains were last exposed to sunlight (i.e., the time of sediment deposition), we stimulated the light-sensitive (bleachable) component of the red TL signal by heating the grains to 260 °C at a heating rate of 5 °C s^{-1} and then holding them at this temperature for 1000 s. From the resulting isothermal decay of the natural and regenerated red TL signals, we estimated the radiation energy absorbed by the grains since the last bleaching event (the equivalent dose, D_e) using the dual-aliquot protocol (DAP) described in detail by Westaway and Roberts (2006). The regenerated signals were induced in the laboratory using a calibrated $^{90}Sr/^{90}Y$ beta source (as used also for the IRSL and OSL analyses described below). DAP requires two aliquots of each sample: one to estimate the D_e associated with the light-insensitive (heat-reset) TL signal, and another to measure the total TL signal, from which the D_e for the bleachable TL signal is estimated by subtraction. It is important to note that the red TL signal takes much longer to bleach than the more light-sensitive components of the OSL and IRSL signals, so the TL ages should conservatively be viewed as maximum ages, to allow for the possibility that not all of the ~5000 grains on each aliquot had been fully bleached at deposition. In the case of the burnt pebble, the D_e corresponds to the radiation energy absorbed since the pebble was last heated to a sufficiently high temperature (i.e., >400 °C) to empty the relevant electron traps.

For IRSL dating of samples LBS7-40 and LBS7-42, K-feldspar grains were mounted on to stainless-steel discs (~2500 grains per disc), and the equivalent doses obtained from the blue emissions using a single-aliquot regenerative-dose (SAR) protocol. Details of the equipment, experimental design, and conditions used are given in Morwood et al. (2004), and example data are shown in Roberts et al. (2005). These procedures produced the correct dose estimates for aliquots that had been bleached and then given a known dose in the laboratory. Both samples exhibited high rates of "anomalous fading" (Wintle, 1973), which will result in age shortfalls unless corrections are made for the decrease in IRSL signal intensity as a function of time (Huntley and Lamothe, 2001; Huntley and Lian, 2006). We measured the fading rate using the SAR approach of Auclair et al. (2003), but obtained such high decay rates (15–30% fading within 2 days of laboratory irradiation) that the relevant electron traps should have been empty in the natural samples when collected, assuming a linear decrease in IRSL intensity with the logarithm of time (Huntley and Lamothe, 2001). As both samples produced natural IRSL signals, however, the laboratory fading rates cannot be valid over geological timescales. We could not, therefore, reliably correct the IRSL ages for fading using available models, so they should be viewed as minimum ages for sediment deposition. For the same reason, the IRSL age obtained for the burnt pebble (sample LBS7-44) could not be corrected for anomalous fading.

OSL dating was carried out on individual quartz grains, using aluminium discs drilled with a 10 × 10 array of chambers, each of which held a single grain. Between 100 and 500 grains were measured for each sample using the modified SAR protocol of Olley et al. (2004). The ultraviolet emissions were stimulated using a 10mW focussed green (532 nm) laser in linear modulation (LM) mode (Bulur et al., 2002). The procedures and instruments used are the same as those described previously (Olley et al., 2006; Westaway et al., 2007a), and routine tests of SAR protocol performance validated the use of these experimental conditions. Our aim was to isolate the most light-sensitive ("fast") component of the LM-OSL signal (Wintle and Murray, 2006), but the emissions were dominated by the less bleachable ("medium" and "slow") OSL components. Thermal instability of the latter components can result in age underestimations (Singarayer and Bailey, 2003; Li and Li, 2006), so the "maximum age model" (Olley et al., 2006) was applied to the distribution of measured single-grain D_e values to estimate the D_e associated with the least-affected grains. Before running the model, a relative uncertainty of 10% was added in quadrature to each D_e measurement error to represent, for well-bleached grains of quartz of equivalent age, the spread in D_e values remaining after taking measurement uncertainties into account. The luminescence signals, methods of D_e determination, and age models currently used to date sediments are reviewed by Lian and Roberts (2006) and, for individual grains of quartz from archaeological deposits, by Jacobs and Roberts (2007).

Luminescence ages are determined by dividing the sample D_e by the dose rate, the latter being the rate of supply of ionizing radiation to the quartz grains from all environmental sources. These include beta and gamma dose rates associated with the radioactive decay of ^{238}U, ^{235}U, and ^{232}Th (and their "daughter" products), ^{40}K and ^{87}Rb, as well as a small contribution from cosmic rays. There is also a significant beta dose rate from ^{40}K and ^{87}Rb present within sand-sized grains of K-feldspar, and U and Th are commonly present at low concentrations inside quartz grains, giving rise to a small internal dose rate. The gamma dose rates were estimated from U, Th, and K concentrations measured in the field with a portable gamma-ray spectrometer, whereas the beta dose rates were obtained from the activities of ^{238}U, ^{235}U, ^{232}Th (and their decay products), and ^{40}K in sediment samples that were dried and powdered in the laboratory and then analyzed using high-resolution gamma-ray spectrometry (Olley et al., 1996, 1997). The latter analyses permitted an assessment of the present-day equilibrium status of the ^{238}U and ^{232}Th decay chains, while the field measurements ensured that any spatial variations in the gamma dose rate were taken into account. The dry dose rates were estimated from these radionuclide activities using the conversion factors of Stokes et al. (2003) and the beta-dose attenuation factors of Mejdahl (1979). Internal dose rates of 0.72 ± 0.09 Gy ka^{-1} and 0.03 ± 0.01 Gy ka^{-1} were assumed for the K-feldspar grains (0.66 Gy ka^{-1} from K and Rb, and 0.06 Gy ka^{-1} from U and Th) and quartz grains, respectively. The cosmic-ray contribution was estimated from the data of Prescott and Hutton (1994), making

allowance for site altitude and geomagnetic latitude, as well as density and thickness of sediment overburden (and limestone shielding, for the cave samples). The dry beta, gamma-, and cosmic-ray dose rates were adjusted for sample moisture content (Aitken, 1985). Present-day field values ranged from 5% to 22%, but we also took into consideration the likely long-term variations experienced during the entire period of sample burial (see detailed assessment in Westaway, 2006).

Electron spin resonance

We used a combination of ESR and U-series dating to analyze three *Stegodon* teeth, and ESR only to analyze another nine teeth. Tooth fragments and whole molars of juvenile, rather than adult, individuals were preferentially selected for dating, because U absorption by dental tissues of larger teeth can result in a significant self-dose from gamma rays, and this can complicate accurate estimation of an ESR age. Tooth enamel was prepared for ESR dating using the procedures described in Jones et al. (2004). This included initial removal of sediment attached to the enamel, measurement of enamel thickness, and removal of the alpha-irradiated portions juxtaposed by the sediment and dentine. U concentrations in the detached sediments and in the dental tissues were determined using delayed neutron activation, while the sedimentary Th and K concentrations were estimated by instrumental neutron activation. The sediment values were used to calculate the external beta dose rate to the enamel and, as with luminescence dating, the external gamma dose rate was estimated by *in situ* gamma-ray spectrometry to capture any spatial variations in the gamma radiation field. A cosmic-ray dose rate of 0.038 Gy ka^{-1} was assumed for all samples; this represents <3% of the total dose rate, so any error in its estimation has an insignificant effect on the calculated age. Adjustments for moisture content were made to the sediment dose rates, using the measured (field) values for the gamma contribution and a value of $20 \pm 10\%$ for the beta component. The latter value and its uncertainty are consistent with the range of moisture contents measured for the sediments located closest to the teeth, and accommodate all likely past fluctuations over the period of burial.

The radiation energy absorbed by the enamel samples since they became buried (i.e., the D_e) was determined using natural and laboratory-irradiated aliquots of powdered enamel. The ESR signals at $g = 2.0018$ were measured on a Bruker X-band spectrometer, and radiation doses were given using a calibrated ^{60}Co gamma source (Jones et al., 2004). The D_e values and their associated uncertainties were calculated by fitting a single saturating-exponential function to the dose-response data, with weights inversely proportional to the squares of the ESR intensities (Brumby, 1992). Present-day U concentrations in the dental tissues are high (2.7–20.2 $\mu g\, g^{-1}$ and 40–125 $\mu g\, g^{-1}$ for enamel and dentine, respectively), indicating that substantial U has been absorbed by the teeth since deposition. For such samples, where the history of U uptake (and possibly some loss) is not known, ESR ages are routinely calculated assuming early uptake of U immediately after burial (the EU model) or a steady (linear) rate of uptake over the entire period of burial (the LU model). We calculated both model ages using the ROSY program (Brennan et al., 1999), updated with the beta-dose attenuation factors of Marsh et al. (2002).

Some constraints on the U-uptake history of a tooth can be obtained by combining the enamel D_e and dose-rate data with the apparent ages obtained from $^{230}Th/^{234}U$ dating of the same enamel and the adjacent dentine (Grün et al., 1988; Rink, 1997; Grün, 2006, 2007). This approach exploits the fact that U-series ages are much more sensitive to uranium migration than are ESR ages. The enamel and dentine fractions of three molars were prepared for U-series dating using the methods described in Jones et al. (2004), and the U and Th isotope signals were then measured by multi-collector inductively-coupled plasma mass spectrometry (MC-ICP-MS) in the GEOTOP Laboratory, University of Québec at Montréal. The U-series ages were calculated assuming "closed system" behavior, in which all of the uranium was introduced at the time of tooth deposition. If this assumption were true, then the U-series and EU-ESR ages for the enamel will agree. But if the U-series age is older, then the tooth has evidently been leached of uranium at some (unknown) point in time, and a coupled ESR/U-series age cannot be determined. For samples with closed-system U-series ages younger than their EU-ESR counterparts, a combined age may be obtained using the *p*-value system of Grün et al. (1988): *p* values of 0 and −1 correspond to linear and early U-uptake, respectively, while intermediate values indicate a more complex history of uranium migration. Values much greater than unity occur in cases of recent U-uptake. The *p*-value system will give the youngest possible combined age for a tooth, but is relatively insensitive to the specific U-uptake history if no leaching has occurred (Grün, 2006). We calculated coupled ESR/U-series ages using the DATA program (Grün, 2009).

Results of the dating program

In this section, we make several chronological comparisons, beginning with an assessment of the internal consistency of numerical ages determined using each technique (*within*-method coherence). We then examine the extent of consistency between the ages obtained by the various dating methods (*between*-method coherence), which are mostly based on different physical principles and associated limitations. The different methods, therefore, can be viewed as providing largely independent chronological constraints. But an exact match between alternative age estimates is not necessarily expected because the dated samples may not relate to the same event. For example, younger ages should be obtained for sediments (dated by luminescence) deposited on top of a pre-existing flowstone (dated by U-series), and the same applies to any incorporated fragments of charcoal (dated by ^{14}C) or tooth enamel (dated by ESR) that are not reworked from older deposits.

All of the measured ages available for Liang Bua and the adjacent river terraces are listed in Tables 2–6, together with the supporting data and associated information (e.g., the calibrated results for ^{14}C dating). Some of these age estimates are considered more reliable than others, for the reasons discussed below. To assist with the chronostratigraphic evaluation of the Sector excavations, the mean or median ages obtained by ^{14}C, luminescence, U-series, and coupled ESR/U-series dating, and the EU and LU model ages (shown as ranges) determined using ESR, are plotted in Fig. 3. For clarity of presentation, the uncertainties on these ages are not given in this figure, so it should be read in conjunction with the relevant table.

Radiocarbon dating

All but two of the ^{14}C age determinations have been made on charcoal samples collected from Sectors IV and VII/XI (Table 2). As expected from stratigraphic principles, the calibrated ages generally increase with depth, from a few hundred years in the top 0.3 m of the deposit to almost 20 ka at a depth of 6.5–6.7 m in Sector VII. The ^{14}C chronology therefore straddles the deposits in which LB1 was found, constraining its age to between 19.8 ka and 15.9 ka at the 95% confidence interval (CI) when the 5 samples from between 6.7 m and 4.8 m are taken into consideration. Of these samples, the two closest to LB1 (ANUA-27116 and ANUA-27117) cover a calibrated age range (95% CI) of 19.0–17.1 ka. The ^{14}C ages also enable reasonably tight constraints of 13.4–10.2 ka (95% CI) to be placed on the time of deposition of the white tuffaceous silts derived from volcanic eruptions (Layer N of Morwood et al., 2004, 2005). These

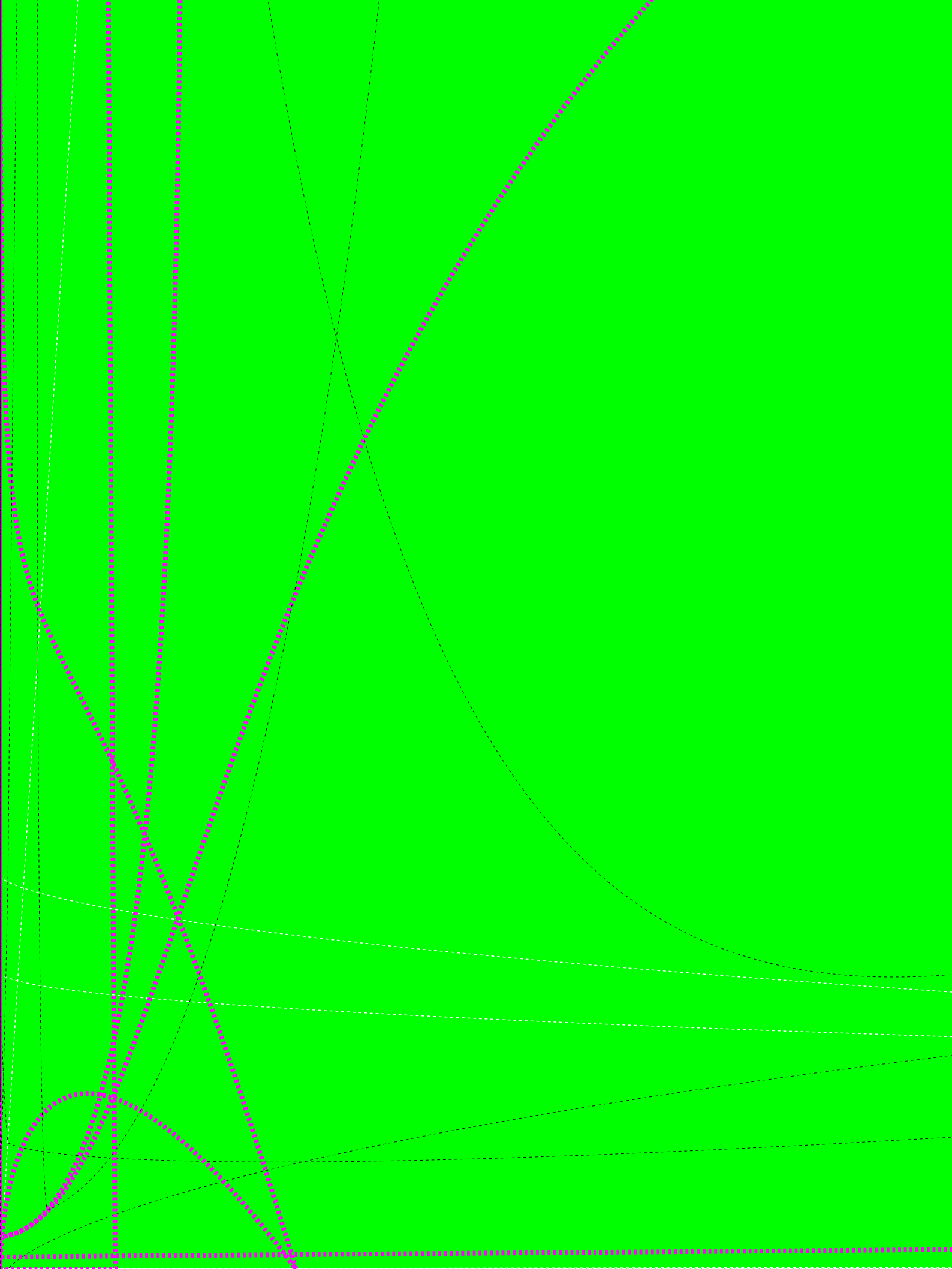

Table 2
Radiocarbon dating of charcoal.

Sample code	Sector/sample depth (cm)	Pre-treatment method (combustion step, °C)/measurement technique[a]	$\delta^{13}C$ value[b] (‰)	Conventional ^{14}C age (yr BP)	Median cal. age[c] (ka)	Cal. 1σ age range[c] (ka)	Cal. 2σ age range[c] (ka)
ANUA-23607	**III**/363	ABOX (850)/AMS	−25.0	1490 ± 210	1.37	1.61–1.14	1.82–0.94
ANUA-23610	**III**/446	ABOX (850)/AMS	−25.0	13,800 ± 230	16.4	16.7–16.0	17.1–15.7
GrN-15870	**IV**/15–25	ABA/GPC	−25.8	190 ± 35	0.14	0.28–0.01	0.28–0.00
GrN-15871	**IV**/25–35	ABA/GPC	−26.0	550 ± 40	0.53	0.55–0.51	0.63–0.50
GrN-14301	**IV**/35–45	ABA/GPC	−26.2	450 ± 25	0.49	0.51–0.47	0.51–0.33
GrN-14302	**IV**/35–45	Acid/GPC	−24.8	580 ± 70	0.57	0.63–0.51	0.66–0.49
GrN-15872	**IV**/45–55	ABA/GPC	−26.3	460 ± 70	0.43	0.53–0.33	0.54–0.31
GrN-14303	**IV**/45–55	Acid/GPC	−25.5	465 ± 35	0.49	0.52–0.47	0.53–0.33
GrN-14304	**IV**/145–155	Acid/GPC	−25.0	3390 ± 270	3.62	3.98–3.26	4.41–2.95
GrN-14305	**IV**/165–175	Acid/GPC	−26.2	3820 ± 120	4.18	4.38–3.98	4.51–3.84
ANUA-19207	**IV**/220–230	ABOX (910)/AMS	−25.0	5620 ± 130	6.37	6.53–6.22	6.67–6.02
GrN-14306	**IV**/305–315	Acid/GPC	−25.0	9830 ± 490	11.3	12.1–10.6	12.8–10.0
ANUA-19206	**IV**/330–340	ABOX (650)/AMS	−25.0	8810 ± 150	9.8	10.1–9.6	10.2–9.5
ANUA-19214	**IV**/330–340	ABOX (910)/AMS	−25.0	8250 ± 160	9.2	9.4–9.0	9.5–8.7
ANUA-19209	**IV**/397–400	ABOX (650)/AMS	−25.0	9640 ± 170	11.0	11.2–10.7	11.4–10.4
ANUA-19211	**IV**/397–400	ABOX (910)/AMS	−25.0	9410 ± 190	10.7	11.1–10.3	11.2–10.2
ANUA-19203	**IV**/480–490	ABOX (650)/AMS	−25.0	13,880 ± 210	16.5	16.8–16.2	17.1–15.8
ANUA-19210	**IV**/480–490	ABOX (910)/AMS	−25.0	13,950 ± 240	16.6	16.9–16.2	17.4–15.9
ANUA-27115	**VII**/450–460	ABOX (650, 850)/AMS	−25.0	11,160 ± 220	13.0	13.2–12.9	13.4–12.7
ANUA-27116	**VII**/588	ABOX (650, 850)/AMS	−25.0	15,300 ± 240	18.5	18.9–18.2	19.0–17.9
ANUA-27117	**VII**/590	ABOX (850)/AMS	−25.0	14,845 ± 240	18.1	18.5–17.7	18.7–17.1
ANUA-31229	**VII**/652	ABOX (850)/AMS	−25.0	15,750 ± 310	19.0	19.3–18.7	19.7–18.2
ANUA-32717	**VII**/670	ABOX (850)/AMS	−25.0	16,130 ± 280	19.2	19.5–19.0	19.8–18.9
Wk-16351	**XI**/20–30	ABA/AMS	−24.8	94 ± 33	0.14	0.25–0.04	0.26–0.03
Wk-16352	**XI**/50–60	ABA/AMS	−25.1	502 ± 32	0.51	0.53–0.50	0.54–0.48
Wk-16353	**XI**/80–90	ABA/LSC	−26.7	2662 ± 35	2.75	2.77–2.73	2.84–2.62
Wk-16354	**XI**/140–150	ABA/AMS	−29.6	4526 ± 39	5.16	5.28–5.05	5.30–4.98
Wk-16355	**XI**/220–230	ABA/AMS	−26.9	7499 ± 47	8.27	8.34–8.20	8.37–8.19

[a] Sample pre-treatments are acid only (Acid), acid–base–acid (ABA), and acid–base wet oxidation (ABOX). The ABOX samples were step-combusted at different temperatures, with the temperature(s) used to obtain the age being shown in parentheses. The techniques used to measure ^{14}C content are gas proportional counting (GPC), liquid scintillation counting (LSC), and accelerator mass spectrometry (AMS).
[b] Value used to make carbon-isotope fractionation correction. Assumed values are shown as −25.0‰; all others are measured values.
[c] Conventional ages have been calibrated using IntCal04 (Reimer et al., 2004), with a Southern Hemisphere offset of 40 ± 13 yr (Hogg et al., 2002), at the 68% (1σ) and 95% (2σ) confidence intervals. The median calibrated age represents the mid-point of the 1σ age range.

a significantly older age (at the 95% CI) was obtained from the 650 °C fraction of the youngest of the ABOX samples step-combusted at both 650 °C and 910 °C (ANUA-19206 and ANUA-19214, respectively). A similar result was obtained for the two separate charcoal samples submitted from a depth of 35–45 cm in Sector IV (GrN-14301 and GrN-14302) by R.P. Soejono; charcoal prepared using only an acid wash gave an older measured age than its counterpart prepared using an ABA pre-treatment, the two values being significantly different at the 68% CI (but not at the 95% CI). The two other available comparisons (between GrN-15872 and GrN-14303, and between ANUA-19209 and ANUA-19211) exhibit the same systematic bias in measured age, but within experimental error. Also, the age of the acid-washed sample from a depth of ~3.1 m (GrN-14306) is significantly older (at the 95% CI) than that obtained for sample ANUA-19214, which was collected from the immediately underlying deposits in Sector IV and given an ABOX pre-treatment prior to combustion at 910 °C. These various comparisons, although not conclusive, suggest that some component of the measured ^{14}C is older than the age of the host charcoal and that the extent of sample contamination by non-elemental carbon compounds can be reduced using ABA or ABOX pre-treatment, together with high-temperature combustion.

Figure 4 is a summary plot of the ^{14}C ages (shown as 95% CI ranges) currently available for Liang Bua, plotted against the depth (below modern ground surface) from which the samples were collected. Only one age is shown for each sample. For the three ABOX samples with two separate step-combustion ages, the age obtained from the highest temperature fraction is displayed. The ages for all of Soejono's acid and ABA pre-treated samples are plotted, as these were obtained from separate charcoal fragments.

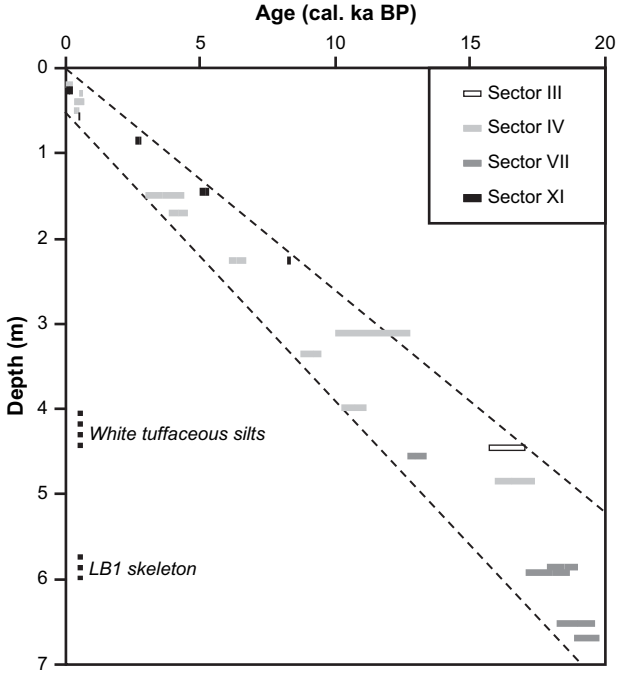

Figure 4. Calibrated ^{14}C age ranges (expressed at the 95% confidence interval in thousands of years before present) for 24 charcoal samples, plotted against the depth (below the modern ground surface) from which the samples were collected; the age of sample ANUA-23607 is not shown. The dashed lines broadly delimit the ages obtained from all four Sectors (III, IV, VII, and XI), which show a general increase of age with depth. In detail, there are differences between sectors, for reasons discussed in the text. The approximate stratigraphic positions (depth intervals) of the LB1 skeleton and white tuffaceous silts are also indicated.

Table 3
Uranium-series dating of calcite speleothems.

Sample location and code[a]	Sample depth[b] (cm)	^{238}U ($\mu g\,g^{-1}$)	^{232}Th ($ng\,g^{-1}$)	$^{230}Th/^{232}Th$ activity ratio	$^{234}U/^{238}U$ activity ratio[c]	$^{230}Th/^{238}U$ activity ratio[c]	Initial $^{234}U/^{238}U$ activity ratio[c]	Uncorrected $^{230}Th/^{234}U$ age[c] (ka)	Corrected $^{230}Th/^{234}U$ age[c,d] (ka)
Sector I									
LB-03-1/45–49	120	0.15	0.34	487	1.027 ± 0.002	0.373 ± 0.002	1.031 ± 0.002	48.9 ± 0.3	48.8 ± 0.3
LB-03-1/7–12	120	0.33	0.14	2941	1.027 ± 0.002	0.399 ± 0.001	1.032 ± 0.002	53.3 ± 0.3	53.3 ± 0.3
LB-03-2/2–13	186	0.16	21.0	10.4	1.023 ± 0.002	0.461 ± 0.007	1.028 ± 0.002	65.0 ± 1.3	61.0 ± 2.4
Sector III									
LB-17-A2/48–52	325	0.10	13.2	17.5	1.028 ± 0.002	0.757 ± 0.008	1.043 ± 0.004	144 ± 3	140 ± 4
LB-17-A2/21–27	325	0.10	29.6	9.65	1.030 ± 0.002	0.917 ± 0.035	1.062 ± 0.007	234 ± 31	225 ± 31
LB-17-A2/3–8	325	0.11	47.0	7.45	1.028 ± 0.002	1.008 ± 0.008	1.091 ± 0.009	386 ± 29	374 ± 30
Sector IV									
LB-JR-6A/13–23	610	0.15	1.01	139	1.027 ± 0.002	0.303 ± 0.001	1.030 ± 0.002	37.9 ± 0.2	37.7 ± 0.2
West wall									
BERT#5	–	0.24	1.69	146	1.035 ± 0.002	0.342 ± 0.002	1.039 ± 0.003	43.5 ± 0.3	43.3 ± 0.3
BERT#6	–	0.24	1.39	69.5	1.026 ± 0.011	0.132 ± 0.002	1.028 ± 0.012	15.0 ± 0.3	14.8 ± 0.3
BERT#7	–	0.19	2.38	104	1.028 ± 0.002	0.431 ± 0.002	1.033 ± 0.003	59.0 ± 0.4	58.6 ± 0.5
Conglomerate cliff									
LB-JR-10A/20–25	–	0.13	1.19	182	1.018 ± 0.002	0.566 ± 0.002	1.023 ± 0.003	87.9 ± 0.6	87.6 ± 0.6
LB-JR-10B/75–80	–	0.14	0.83	307	1.019 ± 0.002	0.603 ± 0.002	1.025 ± 0.003	97.0 ± 0.6	96.8 ± 0.6
LB-JR-10B/3–8	–	0.10	1.25	146	1.014 ± 0.002	0.621 ± 0.002	1.018 ± 0.002	102.8 ± 0.6	102.4 ± 0.6
LB-JR-11A/15–15	–	0.20	101.6	3.75	1.023 ± 0.002	0.631 ± 0.009	1.034 ± 0.004	103.8 ± 2.4	88 ± 9
LB-JR-12/10–15	–	0.28	7.2	51.0	1.023 ± 0.002	0.431 ± 0.002	1.027 ± 0.003	59.3 ± 0.4	58.6 ± 0.5
LB-CON-F2	–	0.19	138.6	2.05	1.055 ± 0.004	0.505 ± 0.006	1.079 ± 0.012	70.3 ± 1.2	47 ± 12
Eroded conglomerate									
LB-CP2-F1-top	–	0.09	2.97	33.2	1.030 ± 0.003	0.365 ± 0.001	1.035 ± 0.003	47.5 ± 0.3	46.5 ± 0.5
LB-CP2-F1-base	–	0.04	4.97	10.3	1.029 ± 0.002	0.391 ± 0.003	1.034 ± 0.002	51.9 ± 0.5	48.5 ± 1.7
LB-CP3-F2-matrix	–	0.16	21.2	8.55	1.027 ± 0.001	0.380 ± 0.002	1.032 ± 0.002	50.2 ± 0.3	46.3 ± 2.0
LB-CP3-F2-clast	–	0.13	3.78	53.9	1.026 ± 0.002	0.522 ± 0.001	1.033 ± 0.002	77.0 ± 0.4	76.2 ± 0.5
Outcrop I									
SPI-1-top	–	0.15	0.60	380	1.024 ± 0.003	0.511 ± 0.002	1.029 ± 0.003	75.0 ± 0.5	74.9 ± 0.6
SPI-1-base	–	0.10	0.66	262	1.014 ± 0.003	0.568 ± 0.003	1.018 ± 0.003	89.0 ± 0.8	88.8 ± 0.8

[a] Sectors I, III, and IV refer to samples collected from the archaeological excavations; "West wall" refers to flowstones attached to the western wall of the cave; "Conglomerate cliff" and "Eroded conglomerate" refer respectively to exposed and buried deposits of fluvial conglomerate at the rear of the cave; and "Outcrop I" refers to a remnant cave situated directly above Liang Bua. See Fig. 1 and Westaway et al. (2009b) for location details.
[b] Below modern ground surface for sector excavations. The West wall, Conglomerate, and Outcrop I samples were collected from higher elevations.
[c] Uncertainties at the 95% confidence interval.
[d] Corrected for the contribution from non-radiogenic (detrital) ^{230}Th, assuming an initial $^{230}Th/^{232}Th$ ratio of $(4.4 \pm 2.2) \times 10^{-6}$ for the non-radiogenic component.

The discrepant age of acid-washed sample GrN-14306 is also shown for completeness, whereas the age of sample ANUA-23607 has been omitted (and is the only such omission). The latter sample has an anomalously young age (1–2 ka) for a depth of ~3.6 m, which we attribute to collection of the charcoal fragments from a deeply incised channel, evident in the east face of Sector III (Fig. 3b).

Sector IV is located ~10 m west of Sectors VII/XI, and Sector III is located a further 5 m to the west, so exact concordance between their age/depth profiles should not be expected. Nonetheless, there is a coherent age structure for the upper ~7 m of stratigraphy in Sectors VII and XI, which are the critical deposits as regards to the LB1 skeleton and associated artifacts, and this extends laterally to the upper ~5 m in Sector IV and possibly Sector III. A uniform sedimentation rate is unlikely to apply to this entire depth interval (or across the entire cave floor), because of the geologically rapid deposition of thick accumulations of the white tuffaceous silts, which are preserved in some (but not all) Sectors at depths of 4–5 m. The upper ~4 m of deposit appears to have accumulated steadily, however, with nearly constant rates of sedimentation during the Holocene of ~35 cm ka^{-1} and ~23 cm ka^{-1} in Sectors IV and XI, respectively (estimated by unweighted linear regression of median calibrated age against depth). The ^{14}C ages show evidence of some mixing of materials in the upper 20–30 cm of deposit (as inferred from the depth-axis intercepts of these linear regressions), possibly extending as deep as 50 cm, which we presume is due to human and other biological activities, including scuffage and treadage of the unconsolidated sediments. This results in imprecise ^{14}C age control for the last ~500 years of the Liang Bua sequence.

Uranium-series dating

In contrast to the ^{14}C samples, only 7 of the 22 speleothem samples were collected from the excavated Sectors at Liang Bua, the most important of these being the flowstone in Sector IV (sample LB-JR-6A/13–23). The majority of samples were collected from flowstones capping the conglomerate cliff at the rear of the cave – where a large stone chopper and a smaller flake were found – and from flowstones formed on top of eroded conglomerate deposits buried at the foot of the cliff (Fig. 1 and Westaway et al., 2007b).

All of the U-series ages reported here include a correction for non-radiogenic ^{230}Th associated with the incorporation of contaminant detritus in the speleothem at the time of formation. Such corrections are not needed for samples with $^{230}Th/^{232}Th$ activity ratios of >1000 (Hellstrom, 2006), but are strongly recommended for samples with ratios of less than ~200 (Richards and Dorale, 2003), which applies to 17 of the 22 speleothem samples. Table 3 lists the $^{230}Th/^{232}Th$ activity ratios, along with the uncorrected and corrected ages, and their estimated uncertainties at the 95% CI. Significant differences in calculated age are apparent for only some samples that have ratios below ~50, but the corrected ages are considered more accurate; henceforth in this paper, we refer exclusively to the latter ages.

Some samples of flowstone were sufficiently thick (several cm) that we could obtain separate ages for superposed layers of calcite crystals and, thus, obtain a microstratigraphic sequence of U-series ages to evaluate their internal consistency. In all cases, the basal layers of flowstone were older than the overlying layer(s), in accord with expectations. For example, two layers of sample LB-03-1 from Sector I were dated individually: crystals located 7–12 mm from the

base of the flowstone were precipitated 53.3 ± 0.3 ka, while the overlying crystals (from 45–49 mm above the base of the flowstone) were formed 48.8 ± 0.3 ka. Correct stratigraphic ordering of ages is also evident in samples LB-17-A2 (from Sector III), LB-JR-10B (from the top of the conglomerate cliff), and LB-CP2-F1 (deposited on top on the now-buried conglomerate shelf extending north from the foot of the conglomerate cliff; Westaway et al., 2007b). The latter site also yielded a flowstone fragment ("clast") with an older U-series age than the surrounding calcitic "matrix" (sample LB-CP3-F2), while the base of a flowstone collected from the remnant cave above Liang Bua ("Outcrop I") gave an older age than did the top. Procedurally, therefore, the results are internally consistent.

These analyses also reveal the highly variable rates of calcite deposition in different flowstones. Sample LB-17-A2 is a large, fallen slab of flowstone found near the center of Sector III. It began forming 374 ± 30 ka and then precipitated a further 45 mm of calcite over the next ~230 ka, which is equivalent to an average accumulation rate of only ~0.2 mm ka^{-1}. Higher rates of calcite deposition of 1–2 orders of magnitude are determined for *in situ* flowstones formed ~100 ka and ~50 ka on top of the conglomerate cliff (LB-JR-10B: ~13 mm ka^{-1}) and in Sector I (LB-03-1: ~8 mm ka^{-1}), respectively.

At a wider spatial scale, the U-series ages are also self-consistent. In Sector I, the two separate pieces of flowstone have ages that are concordant with their relative stratigraphic positions, and the same applies to the three separate chunks of flowstone collected from the top of the conglomerate cliff (sample locations are shown in Westaway, 2006). That is, samples LB-JR-10A and LB-JR-11A have ages of ~88 ka, compatible with them overlying sample LB-JR-10B (~100 ka). The stratigraphic relationship between these three samples and sample LB-JR-12, which is a flowstone also formed on top of the conglomerate cliff but several metres to the west (denoted as U15 in Fig. 1), was not determined in the field, so its calculated age of ~59 ka is not directly comparable with those of the other samples. Only one U-series age clearly falls out of stratigraphic sequence, namely that of sample CON(LB-Con-F2), which was collected from a different position on the cliff face (Westaway et al., 2007b). This thin lens of carbonate capped the basal conglomerate, but required a substantial age-correction for the non-radiogenic ^{230}Th component. We attribute its young age (47 ± 12 ka) to percolation and precipitation of carbonate-enriched waters along the contact between the basal and middle conglomerate layers at ~47 ka. This inferred episode of groundwater movement is consistent with U-series ages of 50–45 ka for the deposition of flowstone on top of the eroded conglomerate shelf that extends downslope from the toe of the cliff (samples LB-CP2-F1 and LB-CP3-F2 "matrix"). At this time, the cliff face ceased to retreat and the remnant conglomerate at its base was sealed by flowstone from further erosion (Westaway et al., 2007b).

At the other end of Liang Bua, close to its entrance, two artifacts were found embedded in a remnant deposit of fluvial conglomerate cemented by carbonate to the west wall of the cave (Fig. 1). Three lenses of crystalline calcite were collected from within 5 cm of the stone tools (a chopper and a large flake). The U-series ages of these samples (BERT#5–7) range from almost 60 ka to ~15 ka, which we interpret as indicating three different episodes of calcite precipitation after deposition of the conglomerate. The earliest episode provides a minimum age for the associated artifacts of 58.6 ± 0.5 ka, which coincides with the timing of flowstone formation in Sector I (sample LB-03-2) and in the conglomerate cliff (sample LB-JR-12); all three sites occur on the western side of the cave. Overall, the U-series chronology provides a coherent framework for cave development and human occupation in the time interval beyond the range of reliable ^{14}C dating.

Luminescence dating

Three types of luminescence signal (TL, OSL, and IRSL) were measured for sediments from inside Liang Bua and from the adjoining sequence of river terraces in the Wae Racang valley. In total, 55 age estimates have been made (Table 4), 29 of which relate to the light-sensitive signals in quartz (bleachable TL – labelled TL-B – and OSL) or K-feldspar (IRSL). The other 26 ages (labelled TL-U in Table 4) were obtained from the unbleachable TL signal, which would have been last reset when the quartz grains were heated to above ~400 °C. This most likely occurred during a volcanic eruption, as the intense orange/red color of the TL emissions is characteristic of volcanic quartz crystallized as phenocrysts at magma temperatures (Rink et al., 1993). Visual inspection of the river terrace sediments also revealed the presence of bipyramidal crystals of (beta) quartz up to 2 mm in size, which are typical of phenocrysts formed in the magma chamber before eruption (Westaway et al., 2007b).

The smaller (90–212 μm diameter) quartz grains dated in this study most likely represent fragments of these phenocrysts (Westaway et al., 2007b). However, because these grains were extracted from cave sediments, and not from *in situ* volcanic deposits, the heat-reset TL ages are unlikely to correspond to the time of the last reworking of these sediment grains. Instead, they give maximum ages for sediment deposition. Accordingly, for the 19 samples that could be dated using both signals, we refer below only to the ages obtained from the bleachable TL signal. For these samples, the unbleachable signal invariably gives an older age than does the bleachable signal, as expected for quartz grains that have been transported several times since their initial crystallization in the magma chamber. The distribution of TL-U ages does not yield a straightforward history of volcanic eruptions because each aliquot was composed of ~5000 grains. There is a high probability, therefore, that each aliquot contained grains that were erupted by many separate events – perhaps spread over hundreds of thousands of years – before being incorporated into the cave and river terrace sediments. Red TL analysis of individual quartz grains (e.g., Yawata and Hashimoto, 2004, 2007) may be able to reveal the timing of discrete volcanic eruptions.

The TL-B ages should probably also be viewed as maximum age estimates for the time of sediment deposition, for two reasons. The first is that the light-sensitive red TL signal requires at least an hour of sunlight exposure to empty the relevant electron traps, and it is not safe to assume that all of the ~5000 grains on each aliquot had been fully bleached when last transported (Westaway and Roberts, 2006). The second is that most of the samples exhibit disequilibria in the ^{238}U decay series, with $^{238}U/^{226}Ra$ ratios of <1; the four most extreme cases fall in the range of 0.24–0.34 (Table 4). Such occurrences have been reported previously for limestone cave deposits, and attributed to the preferential leaching of uranium in association with carbonate complexes (e.g., Olley et al., 1997; Turney et al., 2001). In contrast to U-series dating, however, the loss of uranium does not significantly affect the accuracy of luminescence ages, if (as here) the measured activities of the daughter products are used to determine the dose rates (Olley et al., 1996, 1997). Moreover, higher dose rates (and, hence, younger ages) would be obtained if modelled corrections were made for the uranium deficit, so our recommendation to view the TL ages as maxima is also appropriate for this reason.

There is no evidence to suggest that the luminescence ages will be systematically in error because of disequilibria lower down the ^{238}U decay chain. The weighted mean $^{210}Pb/^{226}Ra$ ratio of 0.94 ± 0.06 for the 17 samples measured by high-resolution gamma-ray spectrometry (Table 4) is consistent with a small (~6%) loss of radon gas to atmosphere, as commonly occurs in

Table 4
Luminescence dating of sediments.

Sample code[a]	Sample depth[b] (m)	Radionuclide activities[c] (Bq kg^{-1})						Field γ dose rate[d] (Gy ka^{-1})	Cosmic-ray dose rate[e] (Gy ka^{-1})	Water content[f] (%)	Total dose rate[g,h] (Gy ka^{-1})	Signal[i]	D_e[g,j] (Gy)	Age[g,k] (ka)
		^{238}U	^{226}Ra	^{210}Pb	^{228}Ra	^{228}Th	^{40}K							
Sector I														
LBS1-16	5.80–5.85	20 ± 3	21.8 ± 0.6	23 ± 3	18.4 ± 1.1	19.1 ± 0.8	109 ± 8	0.227 ± 0.007	0.086	5.6/5 ± 2	1.17 ± 0.06	TL-U	406 ± 21	348 ± 26
												TL-B	61 ± 23	52 ± 20
												OSL (70)	85 $^{+12}/_{-10}$	75 $^{+12}/_{-10}$
LBS1-12	8.40–8.45	–	–	–	–	–	–	0.302 ± 0.009	0.075	20.8/22 ± 5	1.09 ± 0.07	TL-U	479 ± 25	440 ± 36
												TL-B	60 ± 53	55 ± 49
												OSL (67)	92 $^{+10}/_{-12}$	87 $^{+11}/_{-12}$
Sector III														
LBS3-4	4.91–4.96	18.8 ± 0.9	28.9 ± 0.2	34.7 ± 1.3	19.8 ± 0.4	19.3 ± 0.3	128 ± 3	0.272 ± 0.003	0.089	3.0/5 ± 2	1.40 ± 0.05	TL-U	372 ± 19	266 ± 16
												TL-B	96 ± 17	69 ± 12
LBS3-2	7.40–7.45	12.7 ± 0.8	12.4 ± 0.2	14.4 ± 1.0	9.7 ± 0.3	9.4 ± 0.2	101 ± 3	0.286 ± 0.005	0.090	7.7/8 ± 3	0.81 ± 0.04	TL-U	349 ± 13	430 ± 25
												TL-B	86 ± 25	106 ± 31
Sector IV														
LBS4-3	5.00–5.05	–	–	–	–	–	–	0.284 ± 0.004	0.090	11.2/10 ± 4	2.62 ± 0.16	TL-U	185 ± 11	71 ± 6
LBS4-34	5.18–5.23	27.1 ± 0.9	104.7 ± 0.2	70.1 ± 1.1	24.8 ± 0.3	24.1 ± 0.2	57.5 ± 1.2	0.411 ± 0.010	0.089	13.5/14 ± 5	1.67 ± 0.09	TL-U	160 ± 14	96 ± 10
												TL-B	117 ± 12	70 ± 8
LBS4-30	5.45–5.50	9.9 ± 1.4	32.4 ± 0.4	36 ± 2	12.3 ± 0.6	11.7 ± 0.3	56 ± 4	0.205 ± 0.007	0.078	4.6/4 ± 1	1.04 ± 0.04	TL-U	60 ± 4	58 ± 4
												TL-B	15 ± 3	14 ± 3
LBS4-1	6.00–6.05	–	–	–	–	–	–	0.311 ± 0.003	0.085	15.5/15 ± 6	1.54 ± 0.10	TL-U	202 ± 8	131 ± 10
LBS4-26	6.49–6.54	14.3 ± 1.2	18.2 ± 0.2	32.7 ± 1.6	17.3 ± 0.4	17.0 ± 0.3	159 ± 4	0.257 ± 0.001	0.083	3.8/5 ± 2	1.40 ± 0.05	TL-U	344 ± 9	247 ± 11
												TL-B	90 ± 35	65 ± 25
LBS4-28	7.20–7.25	19.1 ± 1.2	28.5 ± 0.2	25.4 ± 1.5	23.2 ± 0.5	23.9 ± 0.3	150 ± 3	0.282 ± 0.002	0.079	22.4/22 ± 6	1.19 ± 0.07	TL-U	351 ± 14	296 ± 21
												TL-B	130 ± 22	110 ± 20
LBS4-32	7.48–7.53	21 ± 2	61.6 ± 0.6	56 ± 3	19.1 ± 0.8	17.8 ± 0.4	40 ± 4	0.300 ± 0.004	0.083	3.4/5 ± 2	1.43 ± 0.06	TL-U	232 ± 10	163 ± 10
												TL-B	136 ± 17	95 ± 13
Sector VII														
LBS7-40	4.85–4.90	35.2 ± 1.9	111.2 ± 0.6	87 ± 3	29.4 ± 0.6	28.9 ± 0.4	48 ± 2	0.596 ± 0.004	0.090	11.3/11 ± 5	2.03 ± 0.12	TL-U	197 ± 8	97 ± 7
												TL-B	81 ± 16	40 ± 8
											2.80 ± 0.11	IRSL	38 ± 6	14 ± 2
LBS7-42	5.93–5.98	31.6 ± 1.9	133.6 ± 0.7	116 ± 4	29.3 ± 0.6	28.5 ± 0.4	29 ± 2	–	0.089	7.9/10 ± 5	2.37 ± 0.14	TL-U	35 ± 8	99 ± 7
												TL-B	86 ± 10	36 ± 5
											3.11 ± 0.12	IRSL	21 ± 2	6.8 ± 0.8
LBS7-44	8.40–8.45	–	–	–	–	–	–	0.356 ± 0.005	0.075	14.5/15 ± 6	1.95 ± 0.13	TL-U	723 ± 300	370 ± 156
											2.64 ± 0.16	IRSL	693 ± 106	263 ± 43
LBS7-46	8.62–8.72	–	–	–	–	–	–	0.529 ± 0.010	0.074	4.8/5 ± 2	1.90 ± 0.08	TL-U	385 ± 26	202 ± 16
												TL-B	78 ± 19	41 ± 10
LBS7-45	9.35–9.40	–	–	–	–	–	–	0.700 ± 0.010	0.071	15.5/15 ± 6	2.78 ± 0.19	TL-U	230 ± 10	93 ± 5
												TL-B	153 ± 21	55 ± 8
Sector XI														
LBS11-50	3.70–3.75	–	–	–	–	–	–	0.207 ± 0.011	0.095	4.7/4 ± 1	1.20 ± 0.06	TL-U	44 ± 25	37 ± 21
Conglomerate cliff														
LBC-37*	1.60–1.65	9.4 ± 1.0	9.7 ± 0.1	2.3 ± 1.4	14.7 ± 0.3	15.0 ± 0.2	305 ± 3	0.288 ± 0.002	0.092	5.7/5 ± 2	1.32 ± 0.05	TL-U	295 ± 10	223 ± 11
												TL-B	172 ± 75	130 ± 57
LBC-36	2.87–2.92	10.9 ± 0.7	9.1 ± 0.1	7.0 ± 0.8	14.2 ± 0.2	13.6 ± 0.2	248 ± 4	0.365 ± 0.005	0.086	5.3/5 ± 2	1.22 ± 0.04	TL-U	325 ± 15	267 ± 16
												TL-B	235 ± 40	193 ± 33
Terrace 3														
WR-9*	1.70–1.75	24 ± 3	30.8 ± 0.4	32 ± 2	36.0 ± 0.8	35.0 ± 0.5	21 ± 3	0.272 ± 0.011	0.191	5.4/7 ± 3	1.41 ± 0.06	TL-U	451 ± 12	340 ± 17
WR-14*	1.80–1.85	28.4 ± 1.5	34.6 ± 0.5	27.1 ± 1.6	43.7 ± 0.8	45.2 ± 0.8	15.6 ± 1.8	0.422 ± 0.006	0.190	5.9/7 ± 3	1.50 ± 0.06	TL-U	321 ± 15	215 ± 13
												TL-B	145 ± 11	97 ± 8
												OSL (44)	201 $^{+33}/_{-18}$	140 $^{+24}/_{-14}$

(*continued on next page*)

Table 4 (*continued*)

Sample code[a]	Sample depth[b] (m)	Radionuclide activities[c] (Bq kg^{-1})						Field γ dose rate[d] (Gy ka^{-1})	Cosmic-ray dose rate[e] (Gy ka^{-1})	Water content[f] (%)	Total dose rate[g,h] (Gy ka^{-1})	Signal[i]	D_e[g,j] (Gy)	Age[g,k] (ka)
		^{238}U	^{226}Ra	^{210}Pb	^{228}Ra	^{228}Th	^{40}K							
WR-15	2.80–2.85	27.0 ± 1.3	32.8 ± 0.4	28.6 ± 1.5	37.0 ± 0.7	37.6 ± 0.6	17.1 ± 1.5	0.340 ± 0.027	0.177	5.6/7 ± 3	1.39 ± 0.06	TL-U	346 ± 16	250 ± 16
												TL-B	164 ± 66	118 ± 48
											1.38 ± 0.06	OSL (39)	130 ± 20	97 $^{+15}/_{-16}$
Terrace 4														
WR-13	1.75–1.80	24.3 ± 1.5	36.9 ± 0.5	30.5 ± 1.7	19.5 ± 0.6	19.6 ± 0.5	45 ± 3	0.267 ± 0.006	0.190	5.1/7 ± 3	1.20 ± 0.05	TL-U	473 ± 29	394 ± 30
												TL-B	21 ± 5	18 ± 4
											1.19 ± 0.05	OSL (50)	42 ± 8	36 ± 7
LB-48	2.04–2.09	–	–	–	–	–	–	0.408 ± 0.010	0.187	6.9/8 ± 3	0.99 ± 0.05	TL-U	602 ± 49	608 ± 58
												OSL (37)	30 ± 5	31 ± 5
LB-47*	4.00–4.05	–	–	–	–	–	–	0.281 ± 0.002	0.164	7.2/7 ± 3	1.06 ± 0.05	TL-U	377 ± 18	356 ± 24
Terrace 5														
WR-1	1.17–1.22	17.2 ± 0.6	24.0 ± 0.1	22.3 ± 0.8	18.9 ± 0.2	19.0 ± 0.1	184 ± 2	0.269 ± 0.008	0.198	6.4/6 ± 2	1.46 ± 0.05	TL-U	337 ± 11	231 ± 11
												TL-B	7 ± 2	5 ± 2
											1.45 ± 0.05	OSL (42)	37 $^{+12}/_{-4}$	26 $^{+9}/_{-3}$

[a] TL samples were processed using the 90–125 μm diameter grain-size fraction, except for those marked with an asterisk (*), which were analyzed using the 125–212 μm fraction. The latter grain-size fraction was also used for all IRSL and OSL analyses.

[b] Depth below modern ground surface for Sector samples; depth below top of cliff for Conglomerate samples; and depth below top of river terrace for Terrace samples.

[c] Activities determined from high-resolution gamma-ray spectrometry measurements of dried and powdered sediment samples. For samples lacking these data, the beta dose rates were determined from the portable gamma-ray spectrometry measurements of individual U, Th, and K concentrations, adjusted for field water content.

[d] Determined from U, Th, and K concentrations measured using a portable gamma-ray spectrometer at field water content.

[e] Time-averaged values for dry samples, assigned relative uncertainties of ±10%.

[f] Field / time-averaged water contents, expressed as (mass of water/mass of dry sample) x 100. The latter values were used to calculate the total dose rates and ages.

[g] Mean ± total uncertainty at 1σ (i.e., 68% confidence interval), calculated as the quadratic sum of the random and systematic uncertainties.

[h] Includes an assumed internal dose rate of 0.03 ± 0.01 Gy ka^{-1} for quartz and 0.72 ± 0.09 Gy ka^{-1} for potassium-rich feldspars.

[i] **TL- U**, unbleachable (heat-reset) red thermoluminescence from quartz; **TL-B**, bleachable (light-reset) red thermoluminescence from quartz; **OSL**, optically-stimulated luminescence from quartz, and (in parentheses) the number of individual grains used to estimate the D_e; **IRSL**, infrared-stimulated luminescence from potassium-rich feldspars.

[j] Equivalent dose (D_e). Uncertainty includes ± 2% systematic component associated with laboratory beta-source calibrations.

[k] IRSL ages are not corrected for anomalous fading.

Table 5
Electron spin resonance (ESR) dating of tooth enamel.

Sample code	Sector/sample depth (cm)	U enamel[a] ($\mu g\,g^{-1}$)	U dentine[a] ($\mu g\,g^{-1}$)	EU age[b] (ka)	LU age[b] (ka)
LB-JR-30A	**I**/160–170	9.6	124.9	22 ± 3	37 ± 4
LB-JR-35A	**IV**/420–430	11.5	106.1	23 ± 3	36 ± 4
LB-JR-9A	**IV**/430–440	8.9	87.5	34 ± 5	57 ± 7
LB-JR-12A	**IV**/440–450	9.4	73.7	32 ± 4	56 ± 7
LB-JR-33A	**IV**/450–460	20.2	76.9	20 ± 1	29 ± 3
LB-JR-8A	**IV**/454	7.5	76.7	54 ± 3	91 ± 5
LB-JR-34A	**IV**/470–480	15.2	63.7	32 ± 1	53 ± 2
LB-JR-14B	**IV**/481	5.3	45.0	58 ± 2	92 ± 4
LB-JR-14D	**IV**/481	8.9	40.0	42 ± 1	69 ± 2
LB-JR-31B	**IV**/500–510	2.7	121.5	36 ± 4	52 ± 6
LB-JR-32A	**IV**/530–540	3.5	98.0	35 ± 3	53 ± 5
LB-JR-15A	**IV**/588	14.1	96.9	40 ± 1	70 ± 2
LB-JR-36A	**VII**/470–480	15.6	60.1	26 ± 1	44 ± 3

[a] Measurement uncertainties of $<0.1\ \mu g\,g^{-1}$.
[b] Early uranium-uptake (EU) and linear uranium-uptake (LU) models. Uncertainties incorporate all sources of random and systematic error. These model ages do not provide meaningful information about the burial time of the teeth, but are listed to enable comparison with the coupled ESR/U-series ages in Table 6.

unconsolidated sediments – including deposits in limestone caves (e.g., Olley et al., 1997; Turney et al., 2001; Prideaux et al., 2007). To estimate the ages, we have assumed that the measured radionuclide activities prevailed throughout the period of sample burial. An unusually small $^{210}Pb/^{226}Ra$ ratio of 0.24 ± 0.14 was measured for sample LBC-37, but increasing this ratio to unity causes a reduction in apparent age of only ~7% (which is much smaller than the total uncertainty on the TL-B age), because the total dose rate is dominated by the contribution from ^{40}K. For all samples, a condition of secular equilibrium currently exists in the ^{232}Th decay series (weighted mean $^{228}Th/^{228}Ra$ ratio of 0.991 ± 0.006), as is typical for terrestrial sediments.

In this study, the OSL ages were determined from D_e measurements on individual grains of quartz, using the "medium" and "slow" OSL components. These are less bleachable than the preferred "fast" component (which was absent in our samples; see Westaway, 2006) and some of the associated electron traps are thermally unstable at typical burial temperatures (Singarayer and Bailey, 2003; Li and Li, 2006). The latter property can give rise to D_e (and, thus, age) underestimates. Unfortunately, a detailed assessment of the presence or absence of the thermally unstable components could not be made on a grain-by-grain basis, owing to their dim OSL signals. Instead, we presumed that the least-affected grains were those that gave the highest D_e values, and determined the corresponding OSL ages using the "maximum age model" (Olley et al., 2006). The calculated ages should also be considered as maxima for another reason: to allow for the possibility that the traps responsible for the medium and slow OSL components were not emptied completely when the sediments were last transported. Hence, the TL and OSL ages both provide a *terminus post quem* for the associated artifacts and faunal remains.

By contrast, the IRSL ages in Table 4 have not been corrected for anomalous fading and, consequently, should be viewed as minimum estimates of the time elapsed since the K-feldspar grains were last exposed to sufficient sunlight (samples LBS7-40 and LBS7-42) or heat (sample LBS7-44) to empty the relevant electron traps. The combination of TL, OSL, and IRSL dating, therefore, provides bracketing age constraints on the time of deposition of the hominin- and artifact-bearing sediments at Liang Bua.

The pattern of TL, OSL, and IRSL ages broadly confirms these expectations. The four TL-B ages in Sector VII (Fig. 3d) are in correct stratigraphic order (within experimental error), and indicate that 10 m of sediment accumulated along the eastern wall of the cave in less than 55 ± 8 ka. The IRSL ages are also younger than their TL counterparts for the two sediment samples collected from above (LBS7-40) and adjacent to (LBS7-42) the *Homo floresiensis* holotype. The bracketing TL and IRSL ages indicate that LB1 was buried by sediments between 36 ± 5 ka and 14 ± 2 ka. The burnt pebble from near the base of Sector VII, however, appears not to have been heated to >400 °C for at least the last 200 ka, based on the TL age obtained for quartz using the heat-reset (unbleachable) signal and the IRSL age for K-feldspar grains extracted from the cortex of the pebble. As the latter age will be too young if any fading has occurred, we cannot reliably estimate the time since last usage of the hearth-like feature from which this pebble was collected (Morwood et al., 2005).

TL-B ages also show good stratigraphic coherence in Sectors I, III, and IV (Fig. 3a–c, respectively), and in the conglomerate cliff at the rear of the cave (Westaway et al., 2007b). The ages in the vicinity of Sectors III and IV correspond to a minimum rate of sediment accumulation of 8 m over the last 95–110 ka, which is less than half the minimum rate in Sectors I and VII (Westaway et al., 2009a). But we caution against the direct comparison of sedimentation rates between Sectors, because the degree to which grains were bleached before deposition may vary in different parts of the cave, depending on the provenance of the grains and the intensity and duration of sunlight exposure that they received. This could give rise to higher maximum ages in some Sectors (e.g., III and IV) than in others (e.g., I and VII).

Two samples from Sector I were dated by both TL and OSL. All four ages are statistically indistinguishable, although the large uncertainties on the TL-B ages preclude an evaluation of which method gives the more accurate estimates. The OSL ages could, in principle, be older than their TL counterparts if the former are

Table 6
Coupled ESR/uranium-series dating of tooth enamel.

Sample code	Sector/sample depth (cm)	$^{234}U/^{238}U$ activity ratio[a]	$^{230}Th/^{234}U$ activity ratio[a]	$^{230}Th/^{232}Th$ activity ratio[a]	Closed system $^{230}Th/^{234}U$ age[a] (ka)	Coupled ESR / $^{230}Th/^{234}U$ age[b] (ka)	*p*-value
LB-JR-8A enamel	**IV**/454	1.033 ± 0.009	0.384 ± 0.005	994 ± 10	52.6 ± 1.0		−0.66 ± 0.21
LB-JR-8A dentine	**IV**/454	1.047 ± 0.013	0.331 ± 0.003	18,778 ± 106	43.6 ± 0.5		−0.39 ± 0.25
						$74\ ^{+14}/_{-12}$	
LB-JR-14B enamel	**IV**/481	1.081 ± 0.005	0.173 ± 0.002	170 ± 2	20.7 ± 0.3		4.9 ± 0.7
LB-JR-14B dentine	**IV**/481	0.975 ± 0.025	0.251 ± 0.016	3458 ± 262	31.4 ± 2.3		2.5 ± 0.6
						$154\ ^{+17}/_{-13}$	
LB-JR-15A enamel	**IV**/588	1.109 ± 0.011	0.542 ± 0.008	3192 ± 32	83.5 ± 1.8		
LB-JR-15A dentine	**IV**/588	1.059 ± 0.027	0.290 ± 0.005	6244 ± 28	37.1 ± 0.8		
						U-loss indicated	

[a] Uncertainties at 95% confidence interval.
[b] Uncertainty incorporates all sources of random and systematic error associated with ESR age determination and 95% confidence limits on the $^{234}U/^{238}U$ and $^{230}Th/^{234}U$ activity ratios for the enamel and dentine.

based on the D_e values from grains dominated by one of the thermally-stable slow components, which take longer to bleach than the light-sensitive red TL signal. Fluvially-transported sediments are commonly bleached incompletely at deposition (e.g., Olley et al., 2004; Singarayer et al., 2005) and should, therefore, exhibit the greatest difference between the TL-B and slow-component OSL ages. The river terrace samples support this suggestion, as the OSL ages for T3, T4, and T5 are significantly older (at the 95% CI) than their respective TL-B ages in three of the four comparisons (Fig. 5). In such circumstances, the TL-B ages are considered more accurate

entirely from the sediments surrounding the tooth, because bone and other tissues deep inside large molars will absorb U, which will give rise to an additional external gamma dose rate that increases with burial time and that needs to be included in the age model.

One of these large molars (LB-JR-14B) shows evidence of recent U-uptake, whereas the other (LB-JR-15A) has suffered from U-loss. For sample LB-JR-14B, $^{230}Th/^{234}U$ ages of ~21 ka and 31 ka were obtained for the enamel and dentine, respectively (Table 6), under the assumption that all of the measured uranium was absorbed immediately after the tooth was buried, after which it remained as a geochemically closed system. The fact that these ages are much younger than the EU-ESR model age (58 ± 2 ka) indicates that U-uptake by the dental tissues was delayed, with the *p*-values being consistent with recent U-absorption. The coupled ESR/U-series age for this tooth ($154\ ^{+17}/_{-13}$ ka) may possibly be correct, but the aforementioned potential complications in accurately estimating the gamma dose rate cast doubt over its reliability. A similarly complex history of uranium migration is also indicated by the closed-system $^{230}Th/^{234}U$ ages of 83.5 ± 1.8 ka (enamel) and 37.1 ± 0.8 ka (dentine) obtained for tooth LB-JR-15A (Table 6). Both of these ages are much older than the EU-ESR age of 40 ± 1 ka (Table 5), which is consistent with recent U-loss from the enamel. This prohibits application of the combined ESR/U-series dating approach and precludes calculation of a meaningful age.

The above examples highlight the difficulty of obtaining tight ESR age constraints for teeth (especially large teeth) deposited in environments where U is mobile and present in high concentration. Owing to the wide differences in U-uptake behavior exhibited by the three teeth investigated for both ESR and U-series dating, we cannot be confident about the U-migration histories of the other samples dated in this study using only ESR. In the absence of coupled U-series measurements, therefore, we consider that the EU and LU model ages for these nine teeth are not informative with regards to their burial age. Accordingly, they are not discussed in the following section. We have reported them here only to provide a complete record of all dating analyses undertaken at Liang Bua, and to illustrate the uncertainties that may accompany ESR ages for teeth collected from similar contexts elsewhere. To estimate the time of deposition of such teeth reliably, U and Th analyses of enamel and dentine must complement ESR measurements, both to test for U-loss and to obtain coupled ESR/U-series ages for any remaining, suitable samples.

Summary and comparison of ages from different methods

In this section, we investigate the between-method coherence of age estimates obtained by ^{14}C, U-series ($^{230}Th/^{234}U$), luminescence (TL, OSL, and IRSL), and coupled ESR/U-series dating. Each of the Sector excavations has multi-method age control, as does the conglomerate cliff deposit at the rear of the cave. The TL, OSL, and IRSL ages are not truly independent of each other, because most of the measured parameters are common to all three luminescence dating methods, which are based on the time-dependent increase in the population of electrons captured by light-sensitive traps in quartz and feldspar crystals. ESR dating of tooth enamel is another trapped-electron-based technique, but the mineral is different (hydroxyapatite) and the electron traps are not light-sensitive. Some components of the dose rate term used in luminescence dating are also shared with ESR dating, but the impact of uranium migration into teeth after burial makes ESR ages far more sensitive to the history of U-uptake and loss than is the case for luminescence dating. Hence, there are a sufficient number of differences between the two methods that they can be considered as semi-independent of each other. Coupled ESR/U-series dating of tooth enamel, perhaps surprisingly, has few problems in common with U-series dating of flowstone. The former approach combines ESR ages with apparent U-series ages obtained for the dental tissues, which are geochemically open systems with regards to uranium migration. By contrast, U-series dating of flowstone gives the time of formation of the calcite crystals, which act as closed systems once sealed from the precipitating groundwaters. In this study, the U-series measurements for the flowstones and dental tissues were also made in different laboratories, thus ensuring that U-series dating of flowstone and coupled ESR/U-series dating of tooth enamel furnish, in effect, completely independent chronologies. The ^{14}C age determinations are fully independent of those obtained by all of the above methods, because trapped electrons and uranium migration are not involved in ^{14}C dating.

Sector I has U-series, TL, and OSL age determinations in stratigraphic sequence (Fig. 3a). The most precise estimates are those obtained for 3 samples of flowstone using $^{230}Th/^{234}U$ dating, which indicate that the upper 2 m of deposit accumulated within the last 50–60 ka. The sediments underlying the flowstone were deposited no earlier than 52 ± 20 ka to 55 ± 49 ka (using the bleachable TL signal) or $75\ ^{+12}/_{-10}$ ka to $87\ ^{+11}/_{-12}$ ka (using OSL). These four luminescence age estimates are statistically indistinguishable, bearing in mind their large uncertainties, and all four are consistent with the U-series ages for flowstone formation. They constrain the time of deposition of the basal sediments in Sector I to the last ~100 ka, which is a feature common also to the nearby Sectors III and IV.

Sector III has age constraints from ^{14}C, U-series, and TL dating that, similarly, are in correct stratigraphic order (Fig. 3b). In this instance, U-series dating was carried out on a fallen slab of flowstone, not a flowstone developed *in situ* in Sector III, so the resultant ages indicate only that the slab of flowstone fell on to the cave floor within the last 140 ± 4 ka and was subsequently buried by ~3 m of deposit. Radiocarbon dating constrains the latter period of sedimentation to the last ~17 ka, while TL dating of the underlying deposits indicates that these accumulated within the last 69 ± 12 to 106 ± 31 ka.

Sector IV is the most intensively dated excavation (Fig. 3c), with a series of thirteen ^{14}C age determinations, two coupled ESR/U-series age estimates, a single U-series age for *in situ* flowstone, and seven TL age estimates (five of which were obtained from the bleachable TL signal). The ^{14}C chronology spans the entire Holocene and the terminal Pleistocene, with only one charcoal sample (95% CI age range of 17.4–15.9 ka) from below the white tuffaceous silts. The ages obtained from the other methods are compatible with the ^{14}C chronology, including the coupled ESR/U-series age of $154\ ^{+17}/_{-13}$ ka for sample LB-JR-14B. As mentioned earlier, this estimate is compromised by the dosimetric complications involved with ESR dating of large, adult molars and should, therefore, conservatively be regarded as a maximum age. This would be consistent with the coupled ESR/U-series age of $74\ ^{+14}/_{-12}$ ka for the overlying juvenile *Stegodon* molar and with the TL-B age of 70 ± 8 ka for the time of deposition of the underlying sediments (sample LBS4-34). The latter two ages are also in accord with the U-series age of 37.7 ± 0.2 ka for the stratigraphically overlying flowstone (sample LB-JR-6A/13–23) and with the ^{14}C chronology for the superposed deposits. The five TL-B ages for the lowermost ~4 m of deposit in Sector IV are similarly in correct stratigraphic order: the youngest age of 14 ± 3 ka was obtained from sediments collected ~1 m below the white tuffaceous silts and ~0.6 m above the flowstone, with the deposits at 7–8 m depth being laid down in the last 110 ± 20 ka. These TL-B ages should be viewed as maximum estimates, although the age of 14 ± 3 ka is statistically consistent with the ^{14}C chronology for the overlying deposits and with the U-series age for the underlying flowstone, which implies that any overestimation of age is not substantial (at least in this

instance). The two ages derived from the unbleachable TL signal (71 ± 6 ka and 131 ± 10 ka) suggests that some recently heated grains were incorporated into the cave sediments during the Late Pleistocene.

Reliable age control for Sectors VII and IX is especially important, as LB1 was excavated from these deposits at a depth of ~6 m (Morwood et al., 2004, 2005). The ^{14}C chronology extends in stratigraphic sequence from a few decades to a few centuries in the upper 30 cm, to almost 20 ka at a depth of 6.7 m (Fig. 3d). Over this depth interval, there are 5 luminescence age estimates. A TL-U age of 37 ± 21 ka was obtained for the Holocene deposits, which indicates only that this sample contains some quartz grains derived from recent volcanic activity (sufficient to reset the high-temperature TL signal). Quartz and K-feldspar grains recovered from the latest Pleistocene deposits, immediately beneath the white tuffaceous silts, produced TL-B and IRSL ages of 40 ± 8 ka and 14 ± 2 ka, respectively. The latter two ages should be viewed as maximum and minimum estimates of the time of sediment deposition above LB1. The IRSL age is indistinguishable from that of the nearest ^{14}C sample (13.4–12.7 ka at the 95% CI), and we note that the TL sample (LBS4-30) collected from a similar stratigraphic position in Sector IV gave a matching, maximum age of 14 ± 3 ka. The ^{14}C and luminescence chronologies, therefore, indicate that the sediment grains and charcoal fragments were deposited contemporaneously ~14 ka, sealing in the holotype of *Homo floresiensis* and the associated artifacts.

Minimum and maximum age estimates of 6.8 ± 0.8 ka (IRSL) and 36 ± 5 ka (TL-B) were obtained for the sediments at the same level as LB1. These ages comfortably bracket the ^{14}C age range (95% CI) of 19.0–17.1 ka for charcoal fragments extracted from the adjacent deposits in which the skeleton was entombed (Morwood et al., 2004). The basal deposits in Sector VII have stratigraphically consistent TL-B ages of 41 ± 10 ka and 55 ± 8 ka, which provide maximum estimates of the time of sediment deposition along the eastern wall of the cave. The TL-U and IRSL ages of >200 ka for sample LBS7-44, from close to the base of Sector VII, indicate that this burnt pebble was not heated to a sufficiently high temperature to empty the relevant electron traps in the near-surface quartz or K-feldspar grains. At the present time, therefore, evidence for the use of fire by *Homo floresiensis* – preserved as charred bone and as clusters of fire-cracked and reddened rocks (Morwood et al., 2005) – is stratigraphically bracketed by TL-B and ^{14}C ages of between ~41 ka and 20 ka.

A final multi-method comparison can be made between the U-series and TL-B ages obtained for the conglomerate cliff at the back of Liang Bua. Ages are, again, in correct stratigraphic order, with the maximum burial ages for the fluvial deposits (130 ± 57 ka and 193 ± 33 ka) being older than the earliest of the flowstones that cap this deposit (102.4 ± 0.6 ka). The only anomaly is the U-series age of 47 ± 12 ka for a thin lens of carbonate collected from between the two TL samples. As discussed above, we attribute its young age to deposition of calcite during a period of groundwater movement at 50–45 ka, when flowstone was also deposited at the top of the cliff (Westaway et al., 2007b).

Throughout this discussion, we have cautioned that the TL ages, even those based on the bleachable TL signal, should conservatively be taken as maximum estimates, to allow for the possibility of incomplete bleaching of the sediments before burial. Partial bleaching will result in grains being deposited with some "inherited" dose remaining from an earlier period of burial, so that the measured D_e will be too large for an aliquot composed of ~5000 grains. Any such effect will exert the greatest bias on the apparent TL ages of sediments deposited recently, because the size of the "inherited" dose will be large relative to the burial dose since the last transport event. The ages of older samples should be less biased, because the D_e will be dominated by the radiation energy absorbed by the grains since the last bleaching event. Fig. 7 shows the five available TL-B ages plotted against reliable, independent age control (provided by ^{14}C, U-series, or coupled ESR/U-series dating). These comparisons suggest that TL-B ages older than ~70 ka provide accurate (i.e., not just maximum) estimates of depositional age. For younger samples, the available data are inconclusive. The youngest sample in Fig. 7 (LBS7-42) has a TL-B age that is significantly older than its ^{14}C counterpart. By contrast, the TL-B age of 14 ± 3 ka for sample LBS4-30 is compatible with the ^{14}C and U-series chronologies for Sector IV, and with the ^{14}C ages obtained at a similar stratigraphic position in Sector VII; its measured D_e of ~15 Gy implies that the "inherited" dose at the time of sediment deposition must have been negligible. Likewise, the D_e value of ~7 Gy and corresponding age of ~5 ka for the stratigraphically youngest of the river terrace samples (WR-1) indicates that the constituent grains had been well-bleached at burial. These findings, and those of Westaway et al. (2007a) for cave breccias in East Java, suggest that the majority of TL-B ages are probably accurate estimates of the time since sediment burial. But our recommendation to treat them as maximum estimates is a more conservative strategy that will accommodate the ages of any partially bleached samples (e.g., LBS7-42), which cannot be identified from any intrinsic features of the light-sensitive red TL signals.

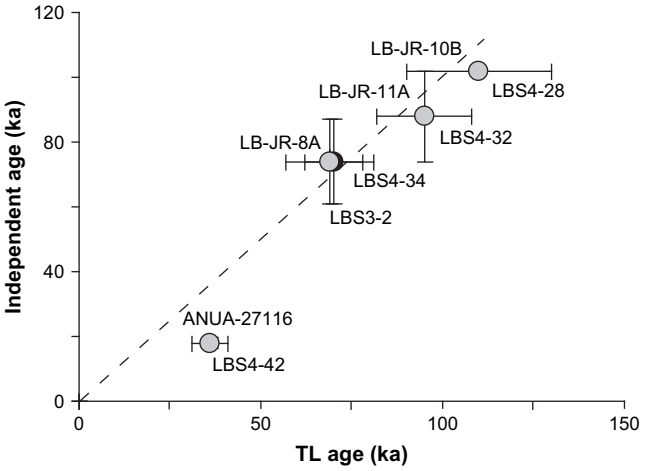

Figure 7. Ages obtained from the bleachable TL signal of 5 samples of quartz, plotted against independent age estimates for associated materials (dated by ^{14}C, U-series, or coupled ESR/U-series). Each point is annotated with the TL sample code on its right and the code of the comparison sample on its left. The dashed line denotes a ratio of unity between the TL and independent age estimates.

Conclusions

No dating technique is without problems, but few sites offer the opportunity to assess the strengths and weaknesses of multiple, alternative chronological approaches. The provision of reliable age control is especially important at Liang Bua because of its palaeoanthropological significance as the type locality of *Homo floresiensis*. This study is a rare example of the parallel application of 7 numerical-age methods (^{14}C, ^{230}Th/^{234}U, TL, OSL, IRSL, ESR, and coupled ESR/U-series) to a variety of materials (charcoal, flowstone, quartz and feldspar grains, and tooth enamel) collected from controlled archaeological excavations. The age estimates provide a series of self-consistent chronologies for the hominin- and artifact-bearing deposits spanning the last ~100 ka. Older stone tools discovered in the fluvial conglomerate deposits at the rear of the cave have also been dated using U-series and TL methods to ~190 ka, when the artifacts were washed into the cave. River

terrace sediments outside the cave have also been dated by TL, providing a Late Pleistocene and Holocene environmental context for hominin activities in the Wae Racang valley (Westaway et al., 2009b). The ages obtained by any particular method show good stratigraphic coherence, while the between-method comparisons are also excellent, taking into account the limitations inherent to each method. As a result, a robust chronological framework has been developed for the archaeological, faunal, and sedimentary sequences at Liang Bua, which is currently the only site at which skeletal remains of *Homo floresiensis* have been found.

Acknowledgements

We thank the Australian Research Council, which funded most of the dating analyses made in this study through grants and/or fellowships to Roberts, Turney, Zhao, and M.J. Morwood. Westaway acknowledges the financial assistance of P. Westaway and the University of Wollongong (University Postgraduate Award and Tuition Fee-Waiver Scholarship). Funding support was also provided by the University of Wollongong (Roberts), the Natural Environment Research Council and Queen's University Belfast (Turney), the Natural Sciences and Engineering Research Council of Canada and McMaster University (Rink), and the University of New England (Morwood). We thank J. Abrantes for assistance with sample preparation for luminescence dating; H. Yoshida and R.M. Bailey for suggestions during development of DAP; D.J. Huntley and O.B. Lian for advice on anomalous fading; J.M. Olley for high-resolution gamma-ray spectrometry measurements; Y.-x. Feng for isotopic measurements for U-series dating of speleothem; and A. Hogg and H. Deenen for providing details of Waikato and Groningen ^{14}C age determinations, respectively.

References

Aitken, M.J., 1985. Thermoluminescence Dating. Academic Press, London.
Aitken, M.J., 1998. An Introduction to Optical Dating: the Dating of Quaternary Sediments by the Use of Photon-stimulated Luminescence. Oxford University Press, Oxford.
Auclair, M., Lamothe, M., Huot, S., 2003. Measurement of anomalous fading for feldspar IRSL using SAR. Radiat. Meas. 37, 487–492.
Bird, M.I., 2007. Charcoal. In: Elias, S.A. (Ed.), Encyclopedia of Quaternary Science. Elsevier, Oxford, pp. 2950–2958.
Bird, M.I., Ayliffe, L.K., Fifield, L.K., Turney, C.S.M., Cresswell, R.G., Barrows, T.T., David, B., 1999. Radiocarbon of "old" charcoal using a wet oxidation, stepped-combustion procedure. Radiocarbon 41, 127–140.
Bird, M.I., Turney, C.S.M., Fifield, L.K., Jones, R., Ayliffe, L.K., Palmer, A., Cresswell, R., Robertson, S., 2002. Radiocarbon analysis of the early archaeological site of Nauwalabila I, Arnhem Land, Australia: implications for sample suitability and stratigraphic integrity. Quat. Sci. Rev. 21, 1061–1075.
Bird, M.I., Fifield, L.K., Santos, G.M., Beaumont, P.B., Zhou, Y., di Tada, M.L., Hausladen, P.A., 2003. Radiocarbon dating from 40 to 60 ka BP at Border Cave, South Africa. Quat. Sci. Rev. 22, 943–947.
Brennan, B.J., Rink, W.J., Rule, E.M., Schwarcz, H.P., Prestwich, W.V., 1999. The ROSY ESR dating program. Ancient TL 17, 45–53.
Brumby, S., 1992. Regression analysis of ESR/TL dose-response data. Nucl. Tracks Radiat. Meas. 20, 595–599.
Bulur, E., Duller, G.A.T., Solongo, S., Bøtter-Jensen, L., Murray, A.S., 2002. LM-OSL from single grains of quartz: a preliminary study. Radiat. Meas. 35, 79–85.
Colman, S.M., Pierce, K.L., Birkeland, P.W., 1987. Suggested terminology for Quaternary dating methods. Quat. Res. 28, 314–319.
Fifield, L.K., Bird, M.I., Turney, C.S.M., Hausladen, P.A., Santos, G.M., di Tada, M.L., 2001. Radiocarbon dating of the human occupation of Australia prior to 40 ka BPdsuccesses and pitfalls. Radiocarbon 43, 1139–1145.
Grün, R., 2006. Direct dating of human fossils. Yrbk. Phys. Anthropol. 49, 2–48.
Grün, R., 2007. Electron spin resonance dating. In: Elias, S.A. (Ed.), Encyclopedia of Quaternary Science. Elsevier, Oxford, pp. 1505–1516.
Grün, R., 2009. The DATA program for the calculation of ESR age estimates on tooth enamel. Quat. Geochron 4, 231–232.
Grün, R., Schwarcz, H.P., Chadam, I., 1988. ESR dating of tooth enamel: coupled corrections for U-uptake and U-series disequilibrium. Nucl. Tracks 14, 237–242.
Grün, R., Maroto, J., Eggins, S., Stringer, C., Robertson, S., Taylor, L., Mortimer, G., McCulloch, M., 2006a. ESR and U-series analyses of enamel and dentine fragments of the Banyoles mandible. J. Hum. Evol. 50, 347–358.
Grün, R., Eggins, S., Wells, R.T., Rhodes, E., Bestland, E., Spooner, N., Ayling, M., Forbes, M., McCulloch, M., 2006b. A cautionary tale from down under: dating the Black Creek Swamp megafauna site on Kangaroo Island, South Australia. Quat. Geochron. 1, 142–150.
Hellstrom, J., 2006. U–Th dating of speleothems with high initial ^{230}Th using stratigraphical constraint. Quat. Geochron. 1, 289–295.
Hogg, A.G., McCormac, F.G., Higham, T.F.G., Reimer, P.J., Baillie, M.G.L., Palmer, J.G., 2002. High-precision radiocarbon measurements of contemporaneous tree-ring dated wood from the British Isles and New Zealand: AD 1850–950. Radiocarbon 44, 633–640.
Huntley, D.J., Lamothe, M., 2001. Ubiquity of anomalous fading in K-feldspars and the measurement and correction for it in optical dating. Can. J. Earth Sci. 38, 1093–1106.
Huntley, D.J., Lian, O.B., 2006. Some observations on the tunnelling of trapped electrons in feldspars and their implications for optical dating. Quat. Sci. Rev. 25, 2503–2512.
Jacobs, Z., Roberts, R.G., 2007. Advances in optically stimulated luminescence dating of individual grains of quartz from archeological deposits. Evol. Anthropol. 16, 210–223.
Jones, H.L., Rink, W.J., Schepartz, L.A., Miller-Antonio, S., Huang, W., Hou, Y., Wang, W., 2004. Coupled electron spin resonance (ESR)/uranium-series dating of mammalian tooth enamel at Panxian Dadong, Guizhou Province, China. J. Archaeol. Sci. 31, 965–977.
Li, B., Li, S.H., 2006. Comparison of D_e estimates using the fast component and the medium component of quartz OSL. Radiat. Meas. 41, 125–137.
Lian, O.B., Roberts, R.G., 2006. Dating the Quaternary: progress in luminescence dating of sediments. Quat. Sci. Rev. 25, 2449–2468.
Marsh, R.E., Prestwich, W.V., Rink, W.J., Brennan, B.J., 2002. Monte Carlo determinations of the beta dose rate to tooth enamel. Radiat. Meas. 35, 609–616.
Mejdahl, V., 1979. Thermoluminescence dating: beta-dose attenuation in quartz grains. Archaeometry 21, 61–72.
Morwood, M.J., Soejono, R.P., Roberts, R.G., Sutikna, T., Turney, C.S.M., Westaway, K.E., Rink, W.J., Zhao, J-x., van den Bergh, G.D., Rokus Awe Due, Hobbs, D.R., Moore, M.W., Bird, M.I., Fifield, L.K., 2004. Archaeology and age of a new hominin from Flores in eastern Indonesia. Nature 431, 1087–1091.
Morwood, M.J., Brown, P., Jatmiko, Sutikna, T., Saptomo, E.W., Westaway, K.E., Rokus Awe Due, Roberts, R.G., Maeda, T., Wasisto, S., Djubiantono, T., 2005. Further evidence for small-bodied hominins from the Late Pleistocene of Flores. Nature 437, 1012–1017.
Morwood, M.J., Sutikna, T., Saptomo, E.W., JatmikoHobbs, D.R., Westaway, K.E., 2009. Preface: research at Liang Bua, Flores, Indonesia. J. Hum. Evol. 57 (5), 437–449.
Olley, J.M., Murray, A., Roberts, R.G., 1996. The effects of disequilibria in the uranium and thorium decay chains on burial dose rates in fluvial sediments. Quat. Sci. Rev. 15, 751–760.
Olley, J.M., Roberts, R.G., Murray, A.S., 1997. Disequilibria in the uranium decay series in sedimentary deposits at Allen's Cave, Nullarbor Plain, Australia: implications for dose rate determinations. Radiat. Meas. 27, 433–443.
Olley, J.M., Pietsch, T., Roberts, R.G., 2004. Optical dating of Holocene sediments from a variety of geomorphic settings using single grains of quartz. Geomorphology 60, 337–358.
Olley, J.M., Roberts, R.G., Yoshida, H., Bowler, J.M., 2006. Single-grain optical dating of grave-infill associated with human burials at Lake Mungo, Australia. Quat. Sci. Rev. 25, 2469–2474.
Prescott, J.R., Hutton, J.T., 1994. Cosmic ray contributions to dose rates for luminescence and ESR dating: large depths and long-term time variations. Radiat. Meas. 23, 497–500.
Prideaux, G.J., Long, J.A., Ayliffe, L.K., Hellstrom, J.C., Pillans, B., Boles, W.E., Hutchinson, M.N., Roberts, R.G., Cupper, M.L., Arnold, L.J., Devine, P.D., Warburton, N.M., 2007. An arid-adapted middle Pleistocene vertebrate fauna from south-central Australia. Nature 445, 422–425.
Reimer, P.J., Baillie, M.G.L., Bard, E., Bayliss, A., Beck, J.W., Bertrand, C.J.H., Blackwell, P.G., Buck, C.E., Burr, G.S., Cutler, K.B., Damon, P.E., Edwards, R.L., Fairbanks, R.G., Friedrich, M., Guilderson, T.P., Hogg, A.G., Hughen, K.A., Kromer, B., McCormac, F.G., Manning, S.W., Ramsey, C.B., Reimer, R.W., Remmele, S., Southon, J.R., Stuiver, M., Talamo, S., Taylor, F.W., Van der Plicht, J., Weyhenmeyer, C.E., 2004. IntCal04 terrestrial radiocarbon age calibration, 26–0 ka BP. Radiocarbon 46, 1029–1058.
Richards, D.A., Dorale, J.A., 2003. Uranium-series chronology and environmental applications of speleothems. In: Bourdon, B., Henderson, G.M., Lundstrom, C.C., Turner, S.P. (Eds.), Uranium-series Geochemistry. Reviews in Mineralogy and Geochemistry, vol. 52. Mineralogical Society of America, Washington, DC, pp. 407–460.
Rink, W.J., 1997. Electron spin resonance (ESR) dating and ESR applications in Quaternary science and archaeometry. Radiat. Meas. 27, 975–1025.
Rink, W.J., Rendell, H.M., Marseglia, E.A., Luff, B.J., Townsend, P.D., 1993. Thermoluminescence spectra of igneous quartz and hydrothermal vein quartz. Phys. Chem. Mineral. 20, 353–361.
Roberts, R.G., Jacobs, Z., 2008. Dating in landscape archaeology. In: David, B., Thomas, J. (Eds.), Handbook of Landscape Archaeology. World Archaeological Congress Research Handbooks in Archaeology, vol. 1. Left Coast Press, Walnut Creek, pp. 347–364.
Roberts, R.G., Morwood, M.J., Westaway, K.E., 2005. Illuminating Southeast Asian prehistory: new archaeological and paleoanthropological frontiers for luminescence dating. Asian Perspect. 44, 293–319.
Singarayer, J.S., Bailey, R.M., 2003. Further investigations of the quartz optically stimulated luminescence components using linear modulation. Radiat. Meas. 37, 451–458.

Singarayer, J.S., Bailey, R.M., Ward, S., Stokes, S., 2005. Assessing the completeness of optical resetting of quartz OSL in the natural environment. Radiat. Meas. 40, 13–25.

Stokes, S., Ingram, S., Aitken, M.J., Sirocko, F., Anderson, R., Leuschner, D., 2003. Alternative chronologies for Late Quaternary (Last Interglacial–Holocene) deep sea sediments via optical dating of silt-sized quartz. Quat. Sci. Rev. 22, 925–941.

Turney, C.S.M., Bird, M.I., Fifield, L.K., Roberts, R.G., Smith, M., Dortch, C.E., Grün, R., Lawson, E., Ayliffe, L.K., Miller, G.H., Dortch, J., Cresswell, R.G., 2001. Early human occupation at Devil's Lair, southwestern Australia 50,000 years ago. Quat. Res. 55, 3–13.

Walker, M., 2005. Quaternary Dating Methods. John Wiley and Sons, Chichester.

Westaway, K.E., 2006. Reconstructing the Quaternary landscape evolution and climate history of western Flores: an environmental and chronological context for an archaeological site. Ph.D. Dissertation, University of Wollongong, Australia.

Westaway, K.E., Roberts, R.G., 2006. A dual-aliquot regenerative-dose protocol (DAP) for thermoluminescence (TL) dating of quartz sediments using the light-sensitive and isothermally stimulated red emissions. Quat. Sci. Rev. 25, 2513–2528.

Westaway, K.E., Morwood, M.J., Roberts, R.G., Rokus, A.D., Zhao, J.-x., Storm, P., Aziz, F., van den Bergh, G., Hadi, P., Jatmiko, de Vos, J., 2007a. Age and biostratigraphic significance of the Punung Rainforest Fauna, East Java, Indonesia, and implications for *Pongo* and *Homo*. J. Hum. Evol. 53, 709–717.

Westaway, K.E., Morwood, M.J., Roberts, R.G., Zhao, J.-x., Sutikna, T., Saptomo, E.W., Rink, W.J., 2007b. Establishing the time of initial human occupation of Liang Bua, western Flores, Indonesia. Quat. Geochron. 2, 337–343.

Westaway, K.E., Sutikna, T., Saptomo, E.W., Jatmiko, Morwood, M.J, Roberts, R.G., Hobbs, D.R., 2009a. Reconstructing the geomorphic history of Liang Bua, Flores, Indonesia: a stratigraphic interpretation of the occupational environment. J. Hum. Evol. 57 (5), 465–483.

Westaway, K.E., Roberts, R.G., Sutikna, T., Morwood, M.J., Drysdale, R., Zhao, J.-x., Chivas, A.R., 2009b. The evolving landscape and climate of western Flores: an environmental context for the archaeological site of Liang Bua. J. Hum. Evol. 57 (5), 450–464.

Wintle, A.G., 1973. Anomalous fading of thermoluminescence in mineral samples. Nature 245, 143–144.

Wintle, A.G., 2007. History of dating methods. In: Elias, S.A. (Ed.), Encyclopedia of Quaternary Science. Elsevier, Oxford, pp. 18–27.

Wintle, A.G., Murray, A.S., 2006. A review of quartz optically stimulated luminescence characteristics and their relevance in single aliquot regeneration dating protocols. Radiat. Meas. 41, 369–391.

Yawata, T., Hashimoto, T., 2004. Identification of the volcanic quartz origins from dune sand using a single-grain RTL measurement. Quat. Sci. Rev. 23, 1183–1186.

Yawata, T., Hashimoto, T., 2007. Development of a red TL detection system for a single grain of quartz. Radiat. Meas. 42, 1460–1468.

Yu, K.-F., Zhao, J.-X., Shi, Q., Chen, T.-G., Wang, P.-X., Collerson, K.D., Liu, T.-S., 2006. U-series dating of dead *Porites* corals in the South China Sea: evidence for episodic coral mortality over the past two centuries. Quat. Geochron. 1, 129–141.

Zhao, J.-x., Hu, K., Collerson, K.D., Xu, H.-k., 2001. Thermal ionization mass spectrometry U-series dating of a hominid site near Nanjing, China. Geology 29, 27–30.